EUROPEAN ORGANIZATION FOR NUCLEAR RESEARCH

Inclusive, prompt and non-prompt J/ψ production at midrapidity in p−Pb collisions at $\sqrt{s_{\mathrm{NN}}} = 5.02$ TeV

ALICE Collaboration[*]

Abstract

A measurement of inclusive, prompt, and non-prompt J/ψ production in p−Pb collisions at a nucleon–nucleon centre-of-mass energy $\sqrt{s_{\mathrm{NN}}} = 5.02$ TeV is presented. The inclusive J/ψ mesons are reconstructed in the dielectron decay channel at midrapidity down to a transverse momentum $p_{\mathrm{T}} = 0$. The inclusive J/ψ nuclear modification factor R_{pPb} is calculated by comparing the new results in p−Pb collisions to a recently measured proton−proton reference at the same centre-of-mass energy. Non-prompt J/ψ mesons, which originate from the decay of beauty hadrons, are separated from promptly produced J/ψ on a statistical basis for p_{T} larger than 1.0 GeV/c. These results are based on the data sample collected by the ALICE detector during the 2016 LHC p−Pb run, corresponding to an integrated luminosity $\mathscr{L}_{\mathrm{int}} = 292 \pm 11 \, \mu\mathrm{b}^{-1}$, which is six times larger than the previous publications. The total uncertainty on the p_{T}-integrated inclusive J/ψ and non-prompt J/ψ cross section are reduced by a factor 1.7 and 2.2, respectively. The measured cross sections and R_{pPb} are compared with theoretical models that include various combinations of cold nuclear matter effects. From the non-prompt J/ψ production cross section, the $\mathrm{b\bar{b}}$ production cross section at midrapidity, $\mathrm{d}\sigma_{\mathrm{b\bar{b}}}/\mathrm{d}y$, and the total cross section extrapolated over full phase space, $\sigma_{\mathrm{b\bar{b}}}$, are derived.

[*]See Appendix A for the list of collaboration members

arXiv:2105.04957v2 [nucl-ex] 7 Dec 2022

1 Introduction

The production of the J/ψ meson in hadronic interactions represents a challenging testing ground for models based on quantum chromodynamics (QCD). In proton$-$proton (pp) and proton$-$antiproton ($p\bar{p}$) collisions, charmonium production has been intensively studied experimentally at the Tevatron [1–4], RHIC [5, 6] and the LHC [7–19], and it can be described in the framework of the non-relativistic quantum chromodynamics (NRQCD) effective theory [20–28].

In heavy-ion collisions, charmonium production is highly sensitive to the nature of the hot and dense matter created in these collisions, the quark$-$gluon plasma (QGP), see Ref. [23, 24, 29] for recent reviews. For a precise interpretation of the heavy-ion results, detailed comparisons with both the reference results obtained in elementary pp collisions and those in proton$-$nucleus (p$-$A) collisions are indispensable. The latter is used to disentangle effects due to interaction between the charmonium states and the QGP medium created in heavy-ion collisions from those that can be ascribed to cold nuclear matter (CNM). In fact, the nuclear environment affects the free nucleon parton distribution functions (PDFs), inducing modifications that depend on the parton fractional momentum x_B, the four-momentum transfer squared (Q^2) and the mass number A, as first discovered by the European Muon Collaboration [30]. The modified distributions can be described using nuclear parton distribution functions (nPDFs) [31–33]. In the x_B and Q^2 domain of "shadowing" reached for nuclear collisions at LHC energies in charm and beauty production, the parton density, and most notably the one of the gluons, is reduced with respect to the free nucleon [34–36]. At very small x_B values, where the gluon density becomes very large, the nuclear environment is expected to favour a saturation process, which can be described using the colour glass condensate (CGC) effective theory [37–39]. In addition, in the nuclear environment partons can lose energy via initial-state radiation, thus reducing the centre-of-mass energy of the partonic system [40], experience transverse momentum broadening due to multiple soft collisions before the production of the pair [41–43], or loose energy through coherent effects [44]. Finally, once produced, the charmonium state could be dissociated via inelastic interactions with the surrounding nucleons [45]. This process, which is dominant among the CNM effects at low collision energy [46, 47], should become negligible at the LHC, where the crossing time of the two nuclei is much shorter than the resonance formation time [48–50].

The comparison of the production measured in p$-$A collisions to the one in pp collisions allows the CNM effects to be constrained. The size of these effects can be quantified by the nuclear modification factor, which is defined as the production cross section in p$-$A collisions (σ_{pA}) divided by that in pp collisions (σ_{pp}) scaled by the mass number A,

$$R_{pA}(y, p_T) = \frac{1}{A} \frac{d^2\sigma_{pA}/dydp_T}{d^2\sigma_{pp}/dydp_T}, \tag{1}$$

where y is the rapidity of the observed hadron in the nucleon$-$nucleon centre-of-mass frame, and p_T its transverse momentum. In the absence of nuclear effects, R_{pA} is expected to be equal to unity.

The inclusive J/ψ yield is composed of three contributions: prompt J/ψ produced directly in the primary hadronic collision, prompt J/ψ produced indirectly via the decay of heavier charmonium states such as χ_c and $\psi(2S)$, and non-prompt J/ψ from the decay of beauty hadrons (h_b). By subtracting the non-prompt component from the inclusive J/ψ production, more direct comparisons with models describing the charmonium production can be considered. However, this contribution is not large, in particular at low p_T ($\approx$ 10–20% for $p_T < 10$ GeV/c [51]), where the bulk of the production is located, and the inclusive J/ψ production represents already a valuable observable.

The measurement of the non-prompt component gives access to study open beauty production through the inclusive decay channel $h_b \rightarrow J/\psi + X$. In pp collisions, the production cross section of beauty hadrons can be computed with factorisation approaches, either in terms of Q^2 (collinear factorisation)

[52] as a convolution of the PDFs of the incoming protons, the partonic hard-scattering cross sections, and the fragmentation functions, or of the partonic transverse momentum k_T [53]. The cold-medium processes that affect the charmonium production in proton$-$nucleus and nucleus$-$nucleus collisions can also affect the beauty hadron production [31–43, 54]. Also in this case, the nuclear modification factor R_{pA} can be useful to study these effects.

Charmonium and open-beauty production cross sections in p$-$Pb collisions have been measured at LHC energies by the ALICE [50, 51, 55–59], ATLAS [14, 60], CMS [15, 61–63] and LHCb [64–67] collaborations over a wide range of rapidity and transverse momentum. Thanks to its moderate magnetic field, particle identification capability, and low material budget of the tracking system in the central barrel, the ALICE apparatus has a unique coverage for J/ψ measurements at midrapidity and low transverse momentum. Previous ALICE measurements were published based on the p$-$Pb data sample collected in 2013 [51, 56, 57, 68]. This paper presents new measurements of the p_T-differential cross sections for the inclusive, prompt, and non-prompt J/ψ production in p$-$Pb collisions at $\sqrt{s_{NN}}$ = 5.02 TeV, using the data sample collected in 2016, which is six times larger than that of 2013. Moreover, the cross section of inclusive J/ψ production measured in pp collisions at $\sqrt{s}$ = 5.02 TeV [7] is used to derive the R_{pA} results instead of the interpolation procedure adopted in the previous p–Pb publication [57]. Therefore, the new results, which are significantly more precise and are obtained differentially in p_T and in finer p_T intervals, supersede the measurements published in Refs. [51, 57].

2 Data Analysis

A complete description of the ALICE apparatus and its performance is presented in Refs. [69, 70]. The central-barrel detectors employed for the analysis presented in this paper are the Inner Tracking System (ITS) and the Time Projection Chamber (TPC). The ITS [71] provides tracking and vertex reconstruction close to the interaction point (IP). It is made up of six concentric cylindrical layers of silicon detectors surrounding the beam pipe with radial positions between 3.9 cm and 43.0 cm. The two innermost layers consist of Silicon Pixel Detectors (SPD), the two central layers are made up of Silicon Drift Detectors (SDD), and the two outermost layers of Silicon Strip Detectors (SSD). The TPC [72] consists of a large cylindrical drift chamber surrounding the ITS and extending from 85 cm to 247 cm along the radial direction and from -250 cm to $+250$ cm along the beam direction (z) relative to the IP. It is the main ALICE tracking device and allows also charged particles to be identified through specific energy loss (dE/dx) measurements in the detector gas. Both the TPC and ITS are embedded in a solenoidal magnet that generates a 0.5 T magnetic field along the beam direction. They cover the pseudorapidity interval $|\eta| < 0.9$ and allow J/ψ mesons to be reconstructed through the e$^+$e$^-$ decay channel in the central rapidity region down to zero p_T.

The measurements presented in this paper are based on the set of minimum bias (MB) p$-$Pb collisions at $\sqrt{s_{NN}}$ = 5.02 TeV collected in 2016 during the LHC Run 2 data taking period, corresponding to an integrated luminosity $\mathscr{L}_{int} = 292 \pm 11\ \mu b^{-1}$. The latter is determined from the number of MB events and the MB-trigger cross section, which was measured via a van der Meer scan, with negligible statistical uncertainty and a systematic uncertainty of 3.7% [73]. Collisions were realized by delivering proton and Pb beams with energies of 4 TeV and 1.58 TeV per nucleon, respectively. The proton and Pb beams circulated in the LHC anticlockwise and clockwise, respectively, during the period of data taking considered for this analysis. The MB trigger condition is provided by the V0 detector [74]: a system made up of two arrays of plastic scintillators placed on either side of the IP and covering the full azimuthal angle and the pseudorapidity intervals $2.8 < \eta < 5.1$ and $-3.7 < \eta < -1.7$. The trigger condition required at least one hit in both the two arrays during the nominal bunch crossing time frame, allowing non-single-diffractive p$-$Pb collisions to be selected with an efficiency higher than 99% [75]. The timing information from the V0 detectors is also used, in combination with that from the SPD, to implement an offline rejection of beam-induced background interactions occurring outside the nominal colliding bunch crossings. Events

with more than one interaction per bunch crossing are reduced down to a negligible amount by means of a dedicated algorithm employing reconstructed tracks to detect the presence of multiple collision vertices. Only collision events with a reconstructed primary vertex lying within ± 10 cm from the nominal IP along the beam direction are considered in order to obtain a uniform coverage for the central-barrel detectors. An event sample of about 6×10^8 MB events is obtained after the application of the above described selection criteria.

2.1 Inclusive J/ψ

Electron candidates are selected following similar procedures as those described in Ref. [57]. The tracks, reconstructed with the ITS and TPC detectors, are required to have a transverse momentum $p_{\mathrm{T}}^{\mathrm{e}} > 1.0$ GeV/c and pseudorapidity $|\eta^{\mathrm{e}}| < 0.9$, as well as at least 70 (out of a maximum of 159) attached TPC clusters and a track fit $\chi^2/\mathrm{dof} < 2$ in order to ensure a uniform tracking efficiency in the TPC. Electron identification is performed by requiring the measured dE/dx to be compatible with the expected specific energy loss for electrons within 3σ, with σ denoting the specific energy-loss resolution of the TPC. Tracks compatible with the pion and proton energy loss expectations within 3σ are rejected. At least one hit in either of the two SPD layers is required to remove background electrons produced from the conversion of photons in the detector materials at large radii. Additional suppression of this background is realized by discarding electron (positron) candidates, which are compatible with a photon conversion when combined with a positron (electron) candidate of the same event, through the application of dedicated topological selections. These selections were verified, employing Monte Carlo (MC) simulations, to have a negligible impact on the J/ψ signal. Finally, in order to reduce the overall background at low transverse momentum, a set of slightly tighter SPD and particle identification (PID) requirements is applied to electrons and positrons forming candidate pairs with $p_{\mathrm{T}} < 3$ GeV/c. A hit in the first SPD layer and a 3.5σ pion and proton rejection condition is required instead of 3σ for higher p_{T} values. The sample of J/ψ candidates is obtained by combining the selected opposite-sign tracks in the same event and requiring the J/ψ rapidity to be within $|y_{\mathrm{lab}}| < 0.9$ in the laboratory system. Due to the energy asymmetry of the proton and lead beams, such a requirement corresponds to a selection of J/ψ candidates within $-1.37 < y < 0.43$ in the nucleon$-$nucleon centre-of-mass system. The resulting dielectron invariant mass ($m_{\mathrm{e^+e^-}}$) distributions are shown in Fig. 1 for eight selected transverse momentum intervals, from 0 to 14 GeV/c. The signal component is characterised by an asymmetric shape, with a long tail towards low invariant masses due to the J/ψ radiative decay channel ($J/\psi \to \mathrm{e^+e^-}\gamma$) and the bremsstrahlung-induced energy loss of daughter electrons in the detector material. The background component is composed of both a combinatorial and a correlated part, with the latter mainly originating from the semileptonic decay of correlated open heavy-flavour hadrons.

The inclusive J/ψ yield is determined from the invariant mass distributions using the same technique as described in Ref. [7]. At first, the combinatorial background shape is modelled by means of a mixed event (ME) technique and then scaled to the invariant mass distribution of like-sign track pairs. Then, the combinatorial background is subtracted from the opposite-sign dielectron invariant mass distribution, and the correlated background is evaluated by fitting the resulting distribution with a two-component function composed of a MC template for the J/ψ signal and of an empirical function for the correlated background. The latter is defined to be either an exponential or a combination of an exponential and a polynomial. The former is obtained by a detailed MC simulation of J/ψ decays in the ALICE detectors, based on GEANT3 [76] and the full reconstruction chain as for real events, which is then also used to correct the raw yield for the selection procedure and detector inefficiencies and described in details in the next paragraph. After subtracting from the opposite-sign dielectron invariant mass distribution also the correlated background, the raw J/ψ yield is obtained by counting the number of entries within the invariant mass interval $2.92 < m_{\mathrm{e^+e^-}} < 3.16$ GeV/c^2. In Fig. 1, the different components used in the procedure to describe the opposite-sign dielectron invariant mass distributions are shown superimposed. An alternative method was also considered, where the invariant mass distribution after the subtraction

of the correlated background is fitted with a Crystal Ball (CB) function [77] for the signal plus either an exponential or a combination of an exponential and a polynomial for the background, and the raw yield is obtained from the integral of the best-fit CB function. The alternative method yields results compatible with those from the standard approach.

In order to correct the raw yield for the chosen selection procedure as well as for detector inefficiencies, a MC simulation was implemented by injecting J/ψ signal events into MB p−Pb collision events simulated with the EPOS-LHC model [78]. The J/ψ component was generated starting with p_T and y distributions that match well a next-to-leading order (NLO) Colour Evaporation Model (CEM) calculations [79, 80] with the inclusion of nuclear effects based on the EPS09 parameterisation [81]. The J/ψ decay into dielectrons was simulated using the EvtGen package [82] in combination with the PHOTOS model [83] in order to provide a proper description of the radiative decay channel. In the simulation, GEANT3 [76] was used to reproduce the propagation of particles through the ALICE experimental setup, taking into account the response of the detectors. The same reconstruction procedure used for data was then applied to the simulated events in order to evaluate the product of acceptance times efficiency ($A \times \varepsilon$), which accounts for: the detector acceptance, the track quality requirements, the electron identification criteria,
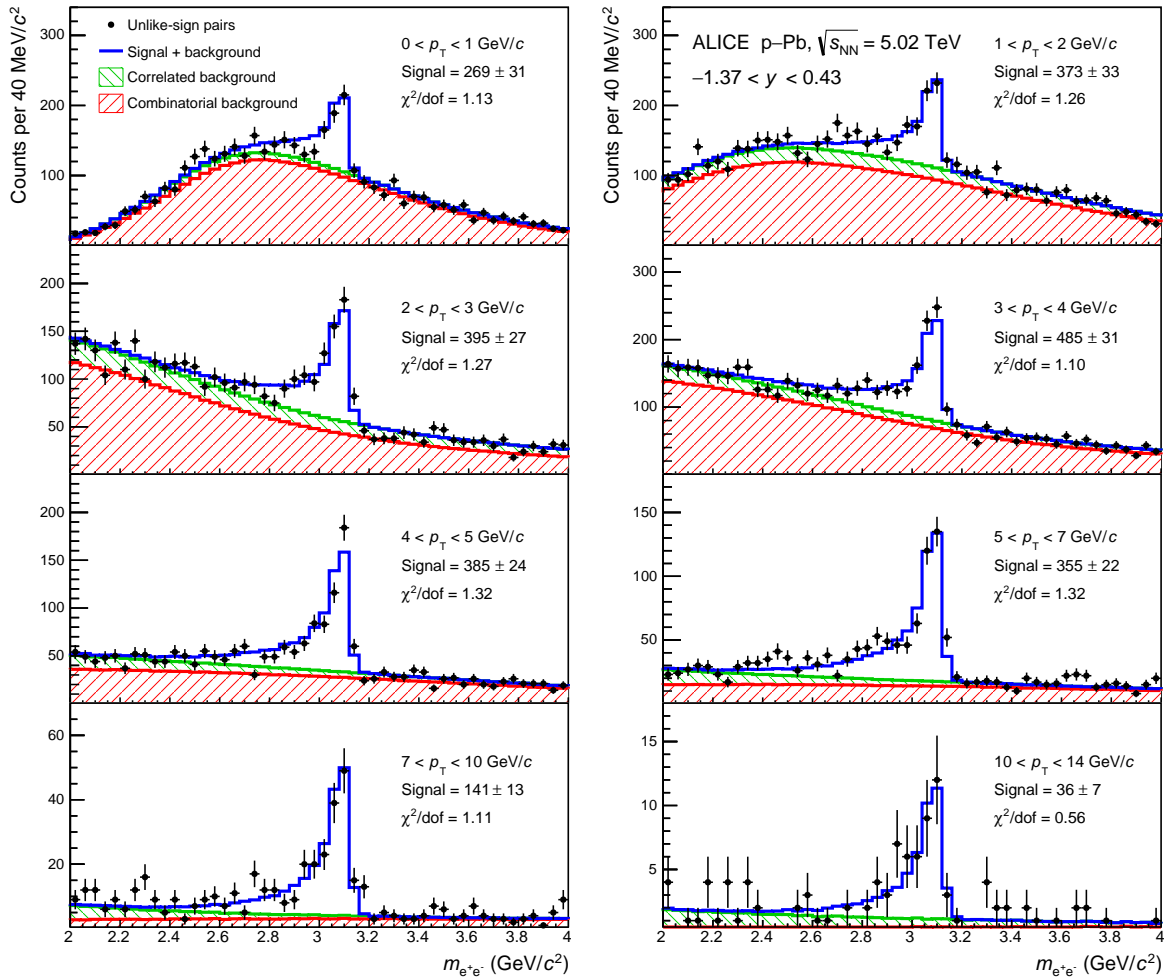

Figure 1: Opposite-sign dielectron invariant mass distributions for the p_T-intervals used for this analysis. The signal plus total background (blue), the combinatorial background (red), and the correlated background (green), evaluated as described in the text, are shown separately in each panel. The χ^2/ndf values of the signal template plus the total background function are also reported along with the raw yields in the range $2.92 < m_{e^+e^-} < 3.16$ GeV/c^2.

and the fraction of the signal counted within the invariant mass interval $2.92 < m_{\mathrm{e}^+\mathrm{e}^-} < 3.16\,\mathrm{GeV}/c^2$. The $A \times \varepsilon$ retrieved from MC exhibits a smooth and mild variation with the J/ψ p_T, ranging from $\sim 8.5\%$ to $\sim 16\%$ in the p_T range from 0 to 14 GeV/c. Consequently, the resulting $\langle A \times \varepsilon \rangle$ correction factor, which is the average of $A \times \varepsilon$ over p_T in a finite-size p_T interval, shows a weak dependence on the p_T shape assumed in the simulation for the J/ψ component. In the end, the final correction factors were computed by re-weighting the original MC distribution to best-fit the inclusive J/ψ spectrum already measured in p–Pb collisions at the same energy [57].

The p_T-differential cross section for inclusive J/ψ production is calculated as

$$\frac{\mathrm{d}^2\sigma_{J/\psi}}{\mathrm{d}y\mathrm{d}p_\mathrm{T}} = \frac{N_{J/\psi}(\Delta y, \Delta p_\mathrm{T})}{\mathrm{BR}\left(J/\psi \rightarrow \mathrm{e}^+\mathrm{e}^-\right) \times \langle A \times \varepsilon \rangle (\Delta y, \Delta p_\mathrm{T}) \times \Delta y \times \Delta p_\mathrm{T} \times \mathscr{L}_{\mathrm{int}}} \ , \tag{2}$$

where $\Delta y = 1.8$ corresponds to the width of the analysed rapidity interval, Δp_T is the width of the considered p_T interval, $N_{J/\psi}$ is the raw J/ψ yield in the interval, and $\mathrm{BR}\left(J/\psi \rightarrow \mathrm{e}^+\mathrm{e}^-\right) = (5.97 \pm 0.03)\%$ is the branching ratio for J/ψ decaying into dielectrons [84].

The inclusive J/ψ nuclear modification factor is obtained, according to Eq. 1, by dividing the p_T-differential cross section by the reference cross section measured up to $p_\mathrm{T} = 10$ GeV/c in pp collisions at $\sqrt{s} = 5.02$ TeV [7]. The rapidity shift of $\Delta y = 0.465$ between the p–Pb and pp samples is expected to introduce a 1% effect on the R_{pPb}, which is negligible with respect to the other uncertainties. An interpolation procedure, which is described in Ref. [51], is adopted for the computation of the reference cross section in the last p_T interval, $10 < p_\mathrm{T} < 14$ GeV/c, that was not measured in pp collisions at this energy. The interpolated value of $\mathrm{d}^2\sigma_{\mathrm{pp}}/\mathrm{d}y\mathrm{d}p_\mathrm{T}$ for this interval amounts to 10 ± 2 nb/(GeV/c), where the quoted uncertainty refers to the total systematic uncertainty arising from the interpolation procedure and is uncorrelated with the uncertainties of the measured $\mathrm{d}^2\sigma_{\mathrm{pp}}/\mathrm{d}y\mathrm{d}p_\mathrm{T}$ for $p_\mathrm{T} < 10$ GeV/c.

The estimated systematic uncertainties affecting the inclusive J/ψ measurements are listed in Table 1. The dominant sources of uncertainty are related to the tracking and electron identification procedures. The remaining contributions are related to the signal extraction procedure, the J/ψ input kinematic distributions used in the MC simulation, the dielectron decay channel branching ratio, and the integrated luminosity determination.

The uncertainty of the tracking procedure dominates at low p_T values and is related to both the ITS-TPC matching efficiency and to the adopted track quality requirements. The first component is estimated by evaluating the discrepancy in the matching probability of TPC tracks to ITS hits between data and Monte Carlo [85]. The observed discrepancy is used to re-scale the tracking efficiency of electrons in MC simulations in order to evaluate the difference in the resulting number of reconstructed J/ψ candidates. The second component is assessed by employing several variations to the adopted track selection criteria and by computing the RMS of the corrected J/ψ yield distribution resulting after these variations. The sum in quadrature of the uncertainties related to both these components is taken as systematic uncertainty on the tracking procedure. The uncertainty related to the electron identification is estimated by evaluating the TPC electron PID response for a clean sample of topologically identified electrons from conversion processes in data and computing the difference with the corresponding quantity from MC simulations. This per-track uncertainty is then propagated to the reconstructed J/ψ candidates with the use of MC simulations. The resulting uncertainty on the J/ψ cross section increases up to $\sim 6\%$ towards high p_T values, where it is the largest uncertainty contribution. The systematic uncertainty related to the signal extraction procedure is due to both the background subtraction and the assumptions on the signal shape. It is estimated as the RMS of the yield distributions corresponding to variations of the mass interval used for the signal counting, the alternative parameterisations employed to fit the correlated background, and the alternative method using the CB function to fit the signal. The uncertainty on the signal shape ranges between $\sim 2\%$ at low p_T and $\sim 2.5\%$ at high p_T, whereas the uncertainty due to the background

Table 1: Summary of the systematic uncertainties, in percentage, of the inclusive J/ψ cross section $\mathrm{d}^2\sigma_{J/\psi}/\mathrm{d}y\mathrm{d}p_T$ and nuclear modification factor R_{pPb} in different p_T intervals. All contributions to the $\mathrm{d}^2\sigma_{J/\psi}/\mathrm{d}y\mathrm{d}p_T$ uncertainty are considered to be highly correlated over the p_T bins, except that for the background subtraction which is considered as fully uncorrelated. The reported values for the measured σ_{pp} reference cross section, which was determined up to $p_T = 10$ GeV/c [7], are the total uncertainties, both of statistical and systematic origins. The uncertainty of σ_{pp} for the interval $10 < p_T < 14$ GeV/c is also the total uncertainty from the interpolation procedure as discussed in the text.

Source	p_T (GeV/c)							
	0–1	1–2	2–3	3–4	4–5	5–7	7–10	10–14
Tracking	4.4	4.4	2.9	2.6	2.6	2.2	2.2	2.7
PID	1.0	1.0	1.2	1.3	1.1	2.1	4.4	6.1
Signal shape	1.9	1.9	1.9	2.1	2.1	2.4	2.4	2.4
Background subtraction	1.9	1.8	2.0	0.9	0.9	0.9	0.9	0.9
MC input	0.1	0.3	0.2	0.2	0.2	0.2	0.7	1.7
σ_{pp}	11.2	9.6	10.5	11.3	12.4	12.8	18.5	22.2
Luminosity	3.7							
Branching ratio	0.5							
Total ($\mathrm{d}^2\sigma_{J/\psi}/\mathrm{d}y\mathrm{d}p_T$)	6.4	6.4	5.6	5.3	5.2	5.5	6.7	8.1
Total (R_{pPb})	12.9	11.5	11.9	12.5	13.4	13.9	19.7	23.7

subtraction varies between ~1% and ~2% and is largest for the lowest p_T intervals. The systematic uncertainty on the J/ψ p_T distribution used as input for the computation of the efficiency corrections is determined by randomly varying, within one standard deviation contour, the parameters of a function fitted to the measured p_T distribution in p$-$Pb collisions [57], taking into account their correlations. The functional form used for this fit is discussed in Ref. [86] and very well describes the measured J/ψ p_T distribution. The uncertainty of the integrated luminosity amounts to 3.7% and is determined from the visible p$-$Pb cross sections measured in van der Meer scans as detailed in Ref. [73]. Both the uncertainty on the integrated luminosity and that on the branching ratio BR $\left(J/\psi \to e^+e^-\right) = (5.97 \pm 0.03)\%$ [84] constitute global uncertainties for the inclusive J/ψ cross section, fully correlated between all p_T intervals. All the other discussed sources of uncertainty are considered to be highly correlated [1] over p_T, with the exception of the background uncertainty, which is considered as uncorrelated.

The total relative uncertainty for the reference pp cross section, σ_{pp}, is also reported in Table 1. In this case, the values up to $p_T = 10$ GeV/c, are the total uncertainties, of both statistical and systematic origin, associated to the measurement performed up to $p_T = 10$ GeV/c [7], while that for the $10 < p_T < 14$ GeV/c interval is the relative uncertainty of the interpolated cross section (10 ± 2 nb/(GeV/c)) quoted before. The uncertainty of σ_{pp} propagates only to the R_{pPb} observable and it varies between ~10% and ~20% and is largest for the highest p_T intervals.

2.2 Determination of the non-prompt J/ψ fraction

The fraction f_b of the J/ψ yield originating from b-hadron decays is measured for $p_T > 1$ GeV/c by discriminating, on a statistical basis, the reconstructed J/ψ candidates according to the displacement between their production vertex and the primary p$-$Pb collision vertex. The discrimination is realized by means of an unbinned two-dimensional likelihood fit, following the same technique adopted in previous analyses for the pp [13], p$-$Pb [51], and Pb–Pb [87] systems. In particular, it is performed by maximising the following log-likelihood function

---

[1] With high correlation, we mean a Pearson coefficient larger than 0.7.

$$\ln L = \sum_1^N \ln \left[f_{\text{Sig}} \times F_{\text{Sig}}(x) \times M_{\text{Sig}}(m_{e^+e^-}) + (1 - f_{\text{Sig}}) \times F_{\text{Bkg}}(x) \times M_{\text{Bkg}}(m_{e^+e^-}) \right] \, , \qquad (3)$$

in which N indicates the number of e^+e^- pairs within the $2.32 < m_{e^+e^-} < 4.00$ GeV/c^2 invariant mass interval. The pseudoproper decay length x is introduced to separate J/ψ originating from the decay of b-hadrons from prompt J/ψ. It is defined as

$$x = \frac{c \times L_{\text{xy}} \times m_{J/\psi}}{p_{\text{T}}} \, , \qquad (4)$$

where c is the speed of light, $L_{\text{xy}} = \vec{L} \cdot \vec{p}_{\text{T}}/p_{\text{T}}$ is the signed projection of the pair flight distance, $\vec{L}$, onto its transverse momentum vector, $\vec{p}_{\text{T}}$, and $m_{J/\psi}$ is the J/ψ pole mass value [84]. The terms F_{Sig} (F_{Bkg}) and M_{Sig} (M_{Bkg}) in Eq. 3 represent the probability density functions (PrDFs) describing the signal (background) pair distributions as a function of x and $m_{e^+e^-}$, respectively, whereas f_{Sig} denotes the ratio of signal to all candidates within the considered mass interval. The signal x PrDF is given by

$$F_{\text{Sig}}(x) = f_b' \times F_b(x) + (1 - f_b') \times F_{\text{prompt}}(x), \qquad (5)$$

with $F_{\text{prompt}}(x)$ and $F_b(x)$ indicating the prompt and non-prompt J/ψ PrDFs, and f_b' being the uncorrected fraction of J/ψ coming from b-hadron decays.

The evaluation of the different PrDFs used in Eq. 3 is performed relying either on data or on MC simulations and following the same procedures described in previous analyses [13, 87]. For the MC simulations, the prompt J/ψ component was generated with the p_{T} and y distributions obtained with a procedure analogue to that previously discussed for the inclusive J/ψ analysis, while the non-prompt J/ψ component was obtained using PYTHIA 6.4 [88] with Perugia-0 tuning [89] to simulate the production of beauty hadrons. Also in this case, the J/ψ decay into dielectrons was simulated using the EvtGen package [82] in combination with the PHOTOS model [83] in order to provide a proper description of the radiative decay channel. The background x PrDF, $F_{\text{Bkg}}(x)$, is determined in three invariant mass ranges by fitting the x distributions of dielectron candidates in the lower ($2.32 < m_{e^+e^-} < 2.68$ GeV/c^2) and upper ($3.20 < m_{e^+e^-} < 4.00$ GeV/c^2) side bands of the invariant mass distributions and by interpolating the resulting fit functions to the region under the invariant mass signal peak ($2.68 < m_{e^+e^-} < 3.20$ GeV/c^2). The experimental resolution function, $R(x)$, which is the key ingredient in the $F_{\text{prompt}}(x)$, $F_b(x)$ and $F_{\text{Bkg}}(x)$ PrDFs, is evaluated from the x distributions of prompt J/ψ in MC simulations, reconstructed after applying the same selection criteria as in data. In order to improve the resolution of the secondary decay vertices, it is required that at least one of the two J/ψ candidate decay tracks has a hit in the innermost SPD layer. A tune-on-data procedure [51] is applied to the MC sample in order to reproduce the observed single-track impact parameter distributions. This minimises the discrepancy between data and simulation, reducing the systematic uncertainty related to the $R(x)$ determination. The $F_b(x)$ PrDF is obtained as the convolution of the $R(x)$ function and a template of the x distribution for the mixture of b-hadrons decaying into J/ψ. The latter is obtained with a MC simulation study of the kinematics of the b-hadron decays. In this simulation, the p_{T}-distribution of the b-hadrons is obtained from pQCD calculations at fixed order with next-to leading-log re-summation (FONLL) [90]. The decay description is based on the EvtGen package [82], and the relative abundance of b-hadron species as a function of p_{T} is based on the precise measurements reported by the LHCb collaboration in pp collisions [91], which are consistent with those measured in p–Pb collisions [67]. The x resolution estimated from the MC simulations is characterised by a pronounced dependence as a function of the J/ψ p_{T}: for events with both J/ψ decay tracks yielding a hit in the first SPD layer, the RMS of the $R(x)$ distribution ranges from $\sim$140 μm at $p_{\text{T}} = 1.5$ GeV/c to $\sim$50 μm at $p_{\text{T}} > 7$ GeV/c. This allows the fraction of non-prompt J/ψ to be determined for events with J/ψ p_{T} greater than 1 GeV/c as well as in five transverse momentum
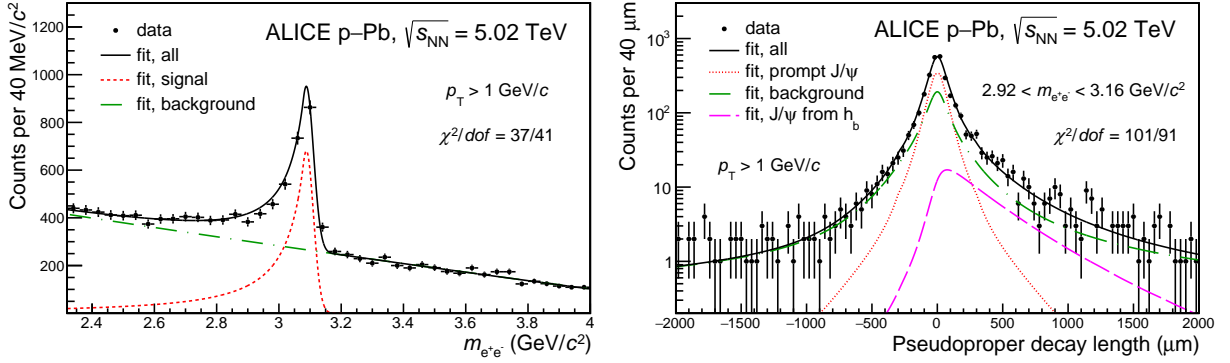
Figure 2: Invariant mass (left panel) and pseudoproper decay length (right panel) distributions for J/ψ candidates with $p_{\mathrm{T}} > 1$ GeV/c. The latter distribution is limited to the J/ψ candidates under the signal peak region $2.92 < m_{\mathrm{e}^+\mathrm{e}^-} < 3.16$ GeV/c^2. The projections of the maximum likelihood fit functions are shown superimposed and the χ^2 values of these projections are also reported for both distributions.

intervals (1–3, 3–5, 5–7, 7–10 and 10–14 GeV/c). The projections of the maximised likelihood fit function superimposed over the $m_{\mathrm{e}^+\mathrm{e}^-}$ and x distributions of J/ψ candidates with $p_{\mathrm{T}} > 1$ GeV/c are shown as an example in Fig. 2.

The f_{b} fraction is obtained after correcting the f_{b}' values (Eq. 6) to account for slightly different $\langle A \times \varepsilon \rangle$ factors of prompt and non-prompt J/ψ:

$$f_{\mathrm{b}} = \left(1 + \frac{1 - f_{\mathrm{b}}'}{f_{\mathrm{b}}'} \times \frac{\langle A \times \varepsilon \rangle_{\mathrm{B}}}{\langle A \times \varepsilon \rangle_{\mathrm{prompt}}} \right)^{-1} . \tag{6}$$

This small correction is computed relying on MC simulations assuming prompt J/ψ to be unpolarised. A small residual polarisation, resulting from the admixture of the different b-hadron decay channels, is assumed for non-prompt J/ψ as predicted by EvtGen [82]. Under these conditions, the correction mainly originates from the difference in the p_{T} distribution between the two components and is found to be significant only for the p_{T}-integrated case. Small relative variations of the corrected f_{b} values, in the order of $\sim$1–4%, are expected in the case of a null-polarisation assumption for non-prompt J/ψ [51]. The variations estimated in extreme polarisation scenarios for prompt J/ψ are discussed in Ref. [13]. Considering the null or very small degree of polarisation measured in pp collisions at the LHC [17, 92–94], these variations are not further propagated to the final results, and only the choice of the p_{T} shapes used as input for the MC simulations is taken into account for the systematic uncertainty evaluation, as discussed below.

The evaluated systematic uncertainties affecting the measurements of f_{b} in the five p_{T} intervals as well as in the p_{T}-integrated range ($p_{\mathrm{T}} > 1$ GeV/c) are listed in Table 2. Most of the listed contributions are due to incomplete knowledge of the different PrDFs used as input for the likelihood fits. An additional contribution originates from the assumptions on the p_{T} distributions employed for the computation of the correction factor of Eq. 6. The uncertainties affecting the evaluation of the resolution function and of the background PrDF constitute the largest contributions to the total systematic uncertainty of the f_{b} measurements. The former is estimated by propagating to the $R(x)$ PrDF the residual discrepancy of the single-track impact parameter distributions between data and MC simulations after the application of the previously discussed tuning procedure. The latter is evaluated by repeating the likelihood fits after varying the procedure used for the determination of the $F_{\mathrm{Bkg}}(x)$ PrDFs, following the same approach described in Ref. [87]. Both uncertainties increase towards low transverse momenta and are largest for the lowest p_{T} interval, where they amount to 10% and 8.5%, respectively. The uncertainty

Table 2: List of the systematic uncertainties (in percent) for the fraction of J/ψ from b-hadron decays in the different analysed p_{T} intervals. The symbol "$-$" denotes a negligible contribution.

Source	p_{T} (GeV/c)					
	>1	1–3	3–5	5–7	7–10	10–14
Resolution function	6.3	10.0	5.5	2.4	1.3	1.1
x PrDF of non-prompt J/ψ	1.7	3.2	0.9	0.5	0.3	0.3
x PrDF of background	5.0	8.5	3.2	3.2	2.6	1.8
Invariant mass PrDF of signal	1.4	1.1	1.3	1.5	1.8	1.8
Invariant mass PrDF of background	1.5	1.8	1.4	1.2	0.8	1.2
Acceptance $\times$ efficiency	3.0	0.3	0.7	0.2	–	–
Total	9.0	13.7	6.7	4.5	3.5	3.0

related to the invariant mass PrDF of the J/ψ signal is estimated by changing the width of the CB function used to parameterise the M_{Sig} PrDF so as to vary the fraction of signal enclosed within the $2.92 < m_{\mathrm{e^+e^-}} < 3.16$ GeV/c^2 interval by $\pm 2.5\%$. The likelihood fits are repeated, and the variation of the resulting f_{b} values is taken as systematic uncertainty. The uncertainty related to the invariant mass background PrDF is estimated as the RMS of the f_{b} value distributions obtained after employing different parameterisations and alternative fitting approaches for the evaluation of the M_{Bkg} PrDF. The estimate of the systematic uncertainty affecting the non-prompt J/ψ x PrDF is performed by repeating the likelihood fits after employing PYTHIA 6.4 for the description of the p_{T}-distribution, decay kinematics, and relative abundance of the beauty hadrons in the MC simulations used to model the $F_{\mathrm{b}}(x)$ PrDF. The relative variation of the resulting f_{b} values, assumed as systematic uncertainty, increases up to $\sim 3\%$ towards low transverse momenta. This uncertainty also contemplates any conservative assumption for a rapidity dependence of the relative abundances of beauty hadrons at the LHC. The uncertainty related to the acceptance times efficiency correction procedure is assessed by testing different hypothesis for the kinematic p_{T}-spectra used to compute the $\langle A \times \varepsilon \rangle$ values that enter into Eq. 6. Among the tested variations, a tune-on-data parameterisation based on the Run 1 measurement [51] for prompt J/ψ, a p_{T}-distribution based on FONLL calculations [90] for the non-prompt component, and the inclusion or exclusion of nuclear shadowing modifications according to the EPPS16 parameterisation [95] are considered. The resulting variations of the correction factors are largest for the p_{T}-integrated measurement, where they amount to $\sim 3\%$, while they are smaller than $\sim 1\%$ within the analysed p_{T}-intervals. The overall systematic uncertainty of the f_{b} measurements is found to increase up to 13.7% towards low transverse momenta, mostly as a consequence of both the increasing combinatorial background and the worsening of the x resolution.

The prompt and non-prompt J/ψ nuclear modification factors are computed by combining the measurements of f_{b} with the previously discussed nuclear modification factors $R_{\mathrm{pPb}}^{\mathrm{incl.\ J/\psi}}$ of inclusive J/ψ:

$$R_{\mathrm{pPb}}^{\text{non-prompt J}/\psi} = \frac{f_{\mathrm{b}}^{\mathrm{pPb}}}{f_{\mathrm{b}}^{\mathrm{pp}}} R_{\mathrm{pPb}}^{\mathrm{incl.\ J/\psi}}, \qquad R_{\mathrm{pPb}}^{\text{prompt J}/\psi} = \frac{1 - f_{\mathrm{b}}^{\mathrm{pPb}}}{1 - f_{\mathrm{b}}^{\mathrm{pp}}} R_{\mathrm{pPb}}^{\mathrm{incl.\ J/\psi}}. \qquad (7)$$

The value of f_{b} in pp collision at $\sqrt{s} = 5.02$ TeV, indicated as $f_{\mathrm{b}}^{\mathrm{pp}}$ in Eq. 7, is determined by means of the same interpolation procedure adopted in previous analyses for the p$-$Pb [51] and Pb$-$Pb [87] systems. The procedure consists of fitting to existing midrapidity f_{b} measurements at $\sqrt{s} = 1.96$ TeV (from CDF [3]) and $\sqrt{s} = 7$ TeV (from ALICE [13], ATLAS [96], and CMS [97]) the semi-phenomenological function discussed in Ref. [87], which includes FONLL predictions [90] for the non-prompt J/ψ production cross section. An energy interpolation is then performed to derive the $f_{\mathrm{b}}^{\mathrm{pp}}(p_{\mathrm{T}})$ at $\sqrt{s} = 5.02$ TeV as a function of p_{T}. The average value of $f_{\mathrm{b}}^{\mathrm{pp}}$ in a given p_{T} interval is obtained by weighting $f_{\mathrm{b}}^{\mathrm{pp}}(p_{\mathrm{T}})$ over the inclusive J/ψ spectrum in pp collisions in that p_{T} interval. Compared to our previous

Table 3: Fraction of non-prompt J/ψ in pp collisions at $\sqrt{s} = 5.02$ TeV computed in different transverse momentum intervals. The reported values and uncertainties are derived following the interpolation procedure detailed in the text and in Ref. [87].

p_{T} (GeV/c)	$f_{\mathrm{b}}^{\mathrm{pp}}$ at $\sqrt{s} = 5.02$ TeV
> 0	0.135 ± 0.013
1–3	0.117 ± 0.013
3–5	0.144 ± 0.012
5–7	0.188 ± 0.014
7–10	0.246 ± 0.019
10–14	0.333 ± 0.038

estimates [51], a tune-on-data spectrum based on the inclusive J/ψ yield measured by ALICE in pp collisions at $\sqrt{s} = 5.02$ TeV [7] is now employed for this purpose. The values of $f_{\mathrm{b}}^{\mathrm{pp}}$ at $\sqrt{s} = 5.02$ TeV, computed in the considered momentum intervals, are reported in Table 3. The quoted uncertainties take into account the uncertainties of both data and FONLL predictions, as well as an additional systematic uncertainty due to the choice of the functional form (either a linear, or an exponential, or a power law function) employed for the energy interpolation procedure.

3 Results

The inclusive J/ψ cross section is measured in $-1.37 < y < 0.43$ both for $p_{\mathrm{T}} > 0$ and differentially in p_{T} considering seven p_{T} intervals, with the first and last bins being $[0-1]$ GeV/c and $[10-14]$ GeV/c, respectively. The value of the p_{T}-integrated inclusive J/ψ cross section per unit of rapidity is dσ/d$y =$ 999 ± 33 (stat.) ± 56 (syst.) μb. The p_{T}-differential cross section of inclusive J/ψ per unit of rapidity, $\mathrm{d}^2\sigma_{\mathrm{incl.J/\psi}}/\mathrm{d}y\mathrm{d}p_{\mathrm{T}}$, is shown in Fig. 3 in comparison with the cross section measured in pp collisions at $\sqrt{s} = 5.02$ TeV [7] multiplied by A $= 208$. The latter extends up to $p_{\mathrm{T}} = 10$ GeV/c. The highest p_{T} point for pp collisions, which is shown in the figure with the empty symbol, was obtained using the interpolation procedure as described before.

The fraction of J/ψ from b-hadron decays in the kinematic range $p_{\mathrm{T}} > 1$ GeV/c and $-1.37 < y < 0.43$, which is referred to as "visible region" in the following, is found to be $f_{\mathrm{b}} = 0.125 \pm 0.017$ (stat.) $\pm$ 0.011 (syst.), where the first quoted uncertainty is statistical and the second one is systematic. The f_{b} measurements in the five analysed p_{T} intervals are shown in Fig. 4 in comparison with our previous results [51] and with the results from the ATLAS collaboration [60], measured for $p_{\mathrm{T}} > 8$ GeV/c within a similar rapidity interval ($-1.94 < y < 0$). The measurements from the CDF [3], ATLAS [98], and CMS [97] experiments in pp and p$\bar{\mathrm{p}}$ collisions at midrapidity are also shown for comparison. With respect to our previous results [51], the present measurements are performed over a wider p_{T} range, with a more granular binning, and show a significantly improved precision, with about half of the statistical uncertainty within similar p_{T} intervals.

The prompt and non-prompt J/ψ production cross sections are obtained from the combination of the f_{b} fractions with the measurements of the inclusive J/ψ cross section $\sigma_{\mathrm{J/\psi}}$:

$$\sigma_{\mathrm{J/\psi \ from \ h_b}} = f_{\mathrm{b}} \times \sigma_{\mathrm{J/\psi}}, \qquad \sigma_{\mathrm{prompt \ J/\psi}} = (1 - f_{\mathrm{b}}) \times \sigma_{\mathrm{J/\psi}}. \tag{8}$$

The non-prompt J/ψ cross section in the visible region, $\sigma_{\mathrm{J/\psi \ from \ h_b}}^{\mathrm{vis}} = 201 \pm 28$ (stat.) ± 21 (syst.) μb, is computed using the inclusive J/ψ cross section for $p_{\mathrm{T}} > 1$ GeV/c, which amounts to 1603 ± 55 (stat.) $\pm$ 89 (syst.) μb.

In order to derive the p_{T}-integrated values of the prompt and non-prompt J/ψ cross section at midrapidity, $\sigma_{\mathrm{J/\psi \ from \ h_b}}^{\mathrm{vis}}$ is extrapolated down to $p_{\mathrm{T}} = 0$ following the approach described in our previous
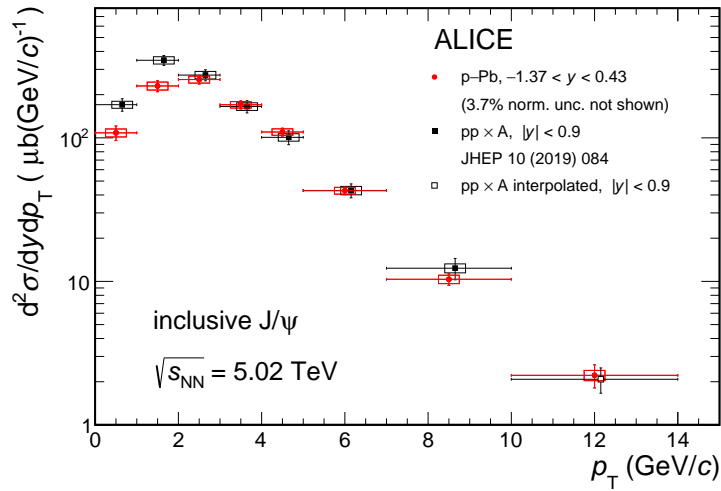
Figure 3: The p_{T}-differential inclusive J/ψ cross section per unit of rapidity, $\mathrm{d}^2\sigma_{\mathrm{incl.}J/\psi}/\mathrm{d}y\mathrm{d}p_{\mathrm{T}}$, as a function of p_{T} in p$-$Pb collisions (red circles) compared with the analogous cross section measured in pp collisions at $\sqrt{s} = 5.02$ TeV [7] multiplied by the Pb mass number (A $= 208$) (black closed squares, shifted horizontally by 150 MeV/c for better visibility). The vertical error bar and the box on top of each point represent the statistical and systematic uncertainty, respectively. The open square symbol (also shifted by 150 MeV/c) shows the value for pp collisions in the p_{T} interval 10-14 GeV/c, which was obtained with the interpolation procedure. In this case the error bar corresponds to the total uncertainty.

work [51]. The extrapolation is performed assuming the shape of the p_{T} distribution of b-quarks obtained from FONLL [90] with the CTEQ6.6 PDFs [99] modified according to EPPS16 nPDF parameterisation [95]. The fragmentation of b-quarks into hadrons is then modelled using PYTHIA 6.4 [88] with the Perugia-0 tune [89]. The ratio of the extrapolated cross section for $p_{\mathrm{T}} > 0$ and $-1.37 < y < 0.43$ to that in the visible region ($p_{\mathrm{T}} > 1$ GeV/c and $-1.37 < y < 0.43$) equals $1.127^{+0.014}_{-0.025}$, where the quoted uncertainty takes into account the FONLL, CTEQ6.6 and EPPS16 uncertainties, as described in Ref. [51], as well as an additional uncertainty, which is related to that on the relative abundance of beauty hadron species in the extrapolated range. The latter is estimated to be about 0.4% after changing the assumed fractions of beauty hadrons according to the recent LHCb measurements [91]. Also, in this case, the considered variation largely includes a possible dependence of these fractions on rapidity. Thus, the measured cross section corresponds to more than 85% of the p_{T}-integrated cross section at midrapidity. Dividing by the rapidity range $\Delta y = 1.8$, the following value is derived for the non-prompt J/ψ cross section per unit of rapidity ($p_{\mathrm{T}} > 0$ and $-1.37 < y < 0.43$):

$$\frac{\mathrm{d}\sigma_{J/\psi \text{ from } h_b}}{\mathrm{d}y} = 125.6 \pm 17.6 \text{ (stat.)} \pm 13.3 \text{ (syst.)} \,^{+1.6}_{-2.8} \text{ (extr.)} \,\mu\text{b}.$$

The corresponding value for the prompt component is obtained as the difference between the inclusive J/ψ cross section, which is measured for $p_{\mathrm{T}} > 0$, and that of J/ψ from b-hadron decays, as determined with the extrapolation procedure described above. It is ($p_{\mathrm{T}} > 0$ and $-1.37 < y < 0.43$)

$$\frac{\mathrm{d}\sigma_{\mathrm{prompt} \, J/\psi}}{\mathrm{d}y} = 873.1 \pm 33.6 \text{ (stat.)} \pm 50.4 \text{ (syst.)} \,^{+1.6}_{-2.8} \text{ (extr.)} \,\mu\text{b}.$$

In Fig. 5 (left panel) this result is shown as a function of rapidity together with the results from the LHCb experiment at positive ("forward") and negative ("backward") rapidity [64], corresponding respectively to the p-going and Pb-going direction. The p_{T}-differential cross section of prompt J/ψ is shown, in comparison with ATLAS measurements [14] at high p_{T} and for $-2 < y < 1.5$, in the right panel of Fig. 5.
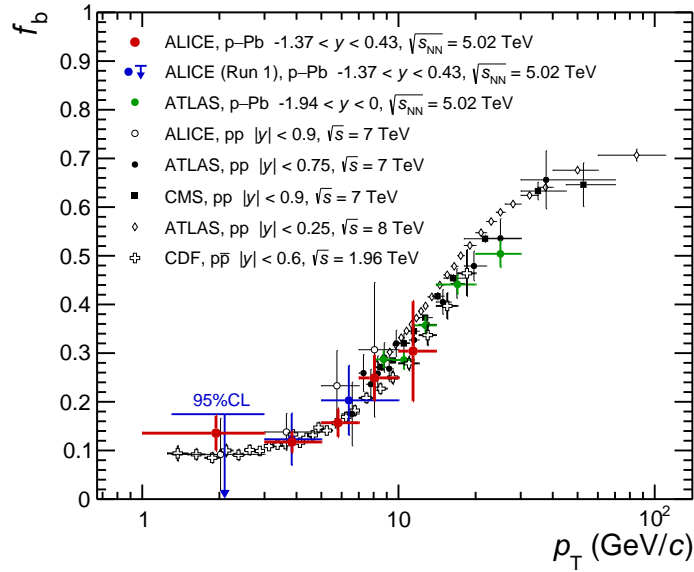
Figure 4: Fraction of J/ψ from b-hadron decays at midrapidity as a function of the J/ψ p_{T} in p–Pb collisions at $\sqrt{s_{\mathrm{NN}}} = 5.02$ TeV (red closed circles) compared with results from the ALICE [51] and ATLAS [60] collaborations in the same collision system (blue and green closed circles, and the blue arrow that shows an upper limit at 95% CL in the range $1.3 < p_{\mathrm{T}} < 3$ GeV/c). The results from CDF [3] in p$\bar{\mathrm{p}}$ collisions at $\sqrt{s} = 1.96$ TeV and those of the ALICE [13], ATLAS [96, 98], and CMS [97] collaborations in pp collisions at $\sqrt{s} = 7$ TeV or $\sqrt{s} = 8$ TeV are also shown (black symbols). For all experiments, vertical error bars represent the quadratic sum of the statistical and systematic uncertainties. The data points of ALICE are placed horizontally at the mean value of the p_{T} distribution within each p_{T}-interval, determined from the MC simulations described in the text.

The ALICE results, covering the low p_{T} region at midrapidity, are complementary to the measurements from both the LHCb and ATLAS collaborations. The data are reported in comparison with model calculations for prompt J/ψ (Lansberg et al. [100–103]) based on the EPPS16 [95] and the nCTEQ15 [104] sets of nuclear parton distribution functions (nPDFs). In both cases, the shaded bands represent the envelope of the computations for different assumptions of the values of the pQCD factorisation (μ_{F}) and renormalisation (μ_{R}) scales (varied within $0.5 < \mu_{\mathrm{F}}/\mu_{\mathrm{R}} < 2$) computed at the 90% confidence level. The predictions show good agreement with data within the large model uncertainties, which are dominated by those on the pQCD scales. The results of a Bayesian reweighting approach from the same authors [101], employing LHCb measurements of J/ψ [66, 105] as a constraint for the computations, are also shown in the left panel of Fig. 5. Both the size of uncertainties and the difference between the nPDF sets are largely reduced after the reweighting.

In Fig. 6, the cross sections of non-prompt J/ψ, computed either for $p_{\mathrm{T}} > 0$ (left panel) or differentially in p_{T} (right panel), are reported together with the corresponding results from the LHCb [64] and AT-LAS [14] collaborations. The results are compared with theoretical predictions based on FONLL pQCD calculations [90] with the inclusion of nuclear shadowing effects according to the EPPS16 nPDFs [95]. In each panel, the coloured curves delimit the total theoretical uncertainty on the production cross section, which is dominated by that of the b-quark mass and the pQCD scales, while the shaded bands refer to the theoretical uncertainty of the EPPS16 nPDFs.

The nuclear modification factor of inclusive J/ψ, measured for $p_{\mathrm{T}} > 0$ and $-1.37 < y < 0.43$, amounts to 0.851 ± 0.028 (stat.) ± 0.079 (syst.). This quantity is obtained using the measured inclusive J/ψ cross section in pp collisions at $\sqrt{s} = 5.02$ TeV [7]. Similarly, the p_{T}-differential R_{pPb} of inclusive J/ψ is obtained on the basis of the measured pp reference, except for the highest p_{T} interval (10–14 GeV/c),
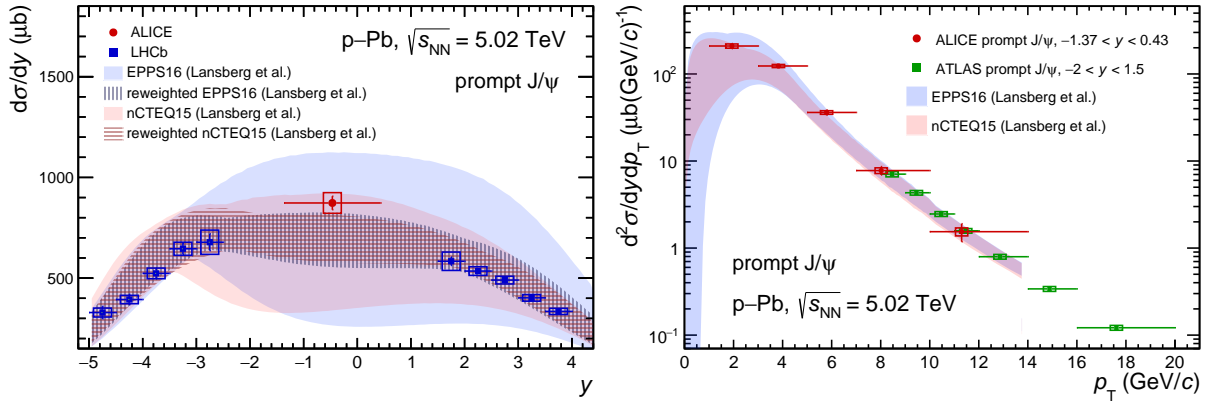
Figure 5: $d\sigma_{\text{prompt } J/\psi}/dy$ as a function of the rapidity in the centre-of-mass frame (left panel) as obtained in this work at midrapidity and by the LHCb collaboration in the forward and backward rapidity regions [64], and $d^2\sigma_{\text{prompt } J/\psi}/dydp_T$ as a function of p_T (right panel) compared with ATLAS results [14] (reported up to $p_T = 20$ GeV/c). The vertical error bars and the boxes on top of each point represent the statistical and systematic uncertainties. In the left panel, the systematic uncertainty of the ALICE data point includes also the contribution from the extrapolation procedure to go from the visible region ($p_T > 1$ GeV/c) to $p_T > 0$, as described in the text. For the measurements as a function of p_T, the data symbols are placed within each bin at the mean of the p_T distribution determined from MC simulations. The results of a model [100–103] including nuclear shadowing based on the EPPS16 [95] and nCTEQ15 [104] nPDFs are shown superimposed on both panels (see text for details). In the right panel, the computations refer only to the ALICE rapidity range.

where the statistical sample is limited and the interpolation procedure [57] is still used. In Fig. 7, the R_{pPb} of prompt J/ψ is reported either for $p_T > 0$ in comparison with LHCb measurements [64] at backward and forward rapidity (left panel) or as a function of p_T, computed according to Eq. 7, together with that of inclusive J/ψ (right panel) in comparison with ATLAS results [14]. The p_T-integrated R_{pPb} of prompt J/ψ at midrapidity ($p_T > 0$ and $-1.37 < y < 0.43$) is measured to be smaller than unity and amounts to 0.860 ± 0.033 (stat.) ± 0.081 (syst.). Given also the relatively small fraction of J/ψ from b-hadron decays for $p_T < 14$ GeV/c, the R_{pPb} of inclusive J/ψ is comparable with that of the prompt component. As shown in the right panel of Fig. 7, both trends indicate that the suppression observed at midrapidity is a low-p_T effect, concentrated for $p_T \lesssim 3$ GeV/c. The measurements are compared with results from various model predictions which embed different CNM effects into prompt J/ψ production. In addition to the previously described computations by Lansberg et al., which include a reweighting of the EPPS16 and nCTE15 nPDFs [101], the central values of a computation based on EPS09 nPDF with or without interaction with a nuclear medium (Ferreiro et al. [106]) are shown. A calculation including the effects of coherent energy loss (Arleo et al. [44]), with or without the introduction of nuclear shadowing effects according to EPS09 nPDF, provides a fairly good description of the measurements either as a function of p_T or as a function of rapidity. Two model calculations based on the CGC effective theory coupled with different elementary production models (Ducloué et al. [107], Ma et al. [108]), are also reported within their domain of validity, in the forward-y region.

The nuclear modification factor for non-prompt J/ψ, determined according to Eq. 7, is shown in Fig. 8. The measured value of the p_T-integrated R_{pPb} for $p_T > 0$ and $-1.37 < y < 0.43$ is found to be 0.79 ± 0.11 (stat.) ± 0.13 (syst.) $^{+0.01}_{-0.02}$ (extr.), suggesting the presence of nuclear effects also for the non-prompt J/ψ component. Within uncertainties, the measurements are found to be compatible with those of the LHCb collaboration [64] at both forward and backward rapidity as well as with those of the ATLAS collaboration [14] for $p_T \gtrsim 9$ GeV/c. All data are in fair agreement with the mild degree of suppression predicted by FONLL computations employing the EPPS16 nPDFs. The nuclear modification factor, as
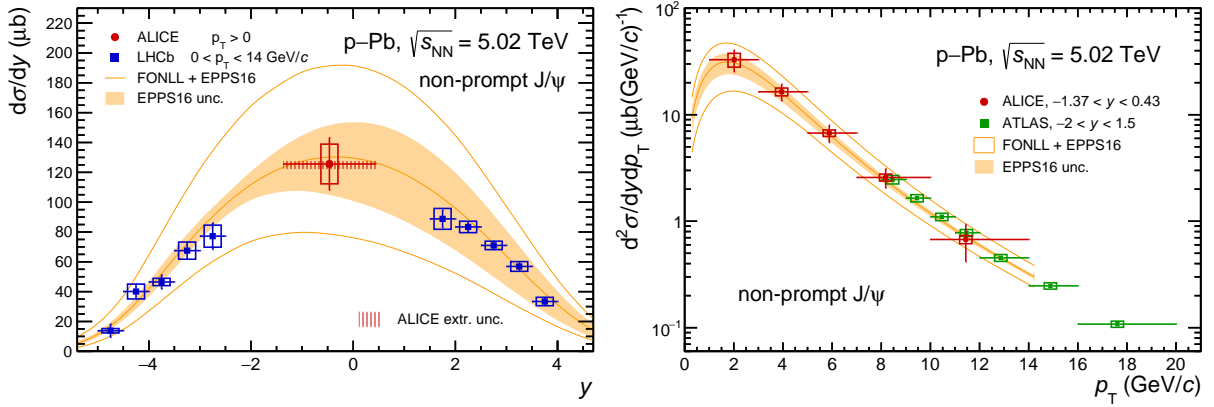
14

Figure 6: $\mathrm{d}\sigma_{J/\psi \text{ from } h_b}/\mathrm{d}y$ as a function of rapidity (left panel) as obtained at midrapidity in this work for $p_T > 0$ and by the LHCb collaboration in the forward and backward rapidity regions [64] for $0 < p_T < 14$ GeV/c, and $\mathrm{d}^2\sigma_{J/\psi \text{ from } h_b}/\mathrm{d}y\mathrm{d}p_T$ as a function of p_T (right panel) compared with ATLAS measurements [14] (shown up to $p_T = 20$ GeV/c). The statistical and systematic uncertainties are shown as vertical error bars and hollow boxes, respectively. The extrapolation uncertainty related to the procedure to go from the visible region ($p_T > 1$ GeV/c) to $p_T > 0$ for the ALICE data point in the left panel is indicated with a dashed band. For the measurements as a function of p_T, data symbols are placed at the mean value of the p_T distribution within each bin. The results are compared to FONLL computations [90] with EPPS16 [95] nPDFs, highlighting the total theoretical uncertainty (empty band) and the contribution from EPPS16 (coloured band). In the right panel, model computations are obtained in the same rapidity range of the ALICE results, namely $-1.37 < y < 0.43$.

predicted from the Bayesian reweighting approach [101] of the EPPS16 nPDFs previously introduced for the prompt component, also provides a good description of the measurements. The central value of an alternative parameterisation of the nuclear PDF, nDSgLO [109], is reported in the left-hand panel. Despite the larger relative uncertainties, the comparison with the results shown for the prompt component (right panel of Fig. 7) suggests that a reduced suppression as well as a less pronounced p_T-dependence affect the component of J/ψ from b-hadron decays.

Similarly as for our previous work [51], the low p_T coverage of the measured non-prompt J/ψ cross section at midrapidity, now extending down to $p_T = 1$ GeV/c, allows the p_T-integrated $b\bar{b}$ cross section per unit of rapidity, $\mathrm{d}\sigma_{b\bar{b}}/\mathrm{d}y$, and the total $b\bar{b}$ production cross section, $\sigma(\mathrm{pPb} \to b\bar{b} + X)$, to be derived with small extrapolation uncertainties. By using FONLL with CTEQ6.6 and EPPS16 nPDFs as input model for the computation of the extrapolation factor, the $b\bar{b}$ production cross section at midrapidity is derived as

$$\frac{\mathrm{d}\sigma_{b\bar{b}}}{\mathrm{d}y} = \frac{\mathrm{d}\sigma_{b\bar{b}}^{\text{model}}}{\mathrm{d}y} \times \frac{\sigma_{J/\psi \text{ from } h_b}^{\text{vis}}}{\sigma_{J/\psi \text{ from } h_b}^{\text{vis, model}}} . \tag{9}$$

Assuming the average branching ratio of J/ψ from b-hadron decays measured at LEP [110–112], $BR(\mathrm{h}_b \to J/\psi + X) = (1.16 \pm 0.10)\%$, for the computation of $\sigma_{J/\psi \text{ from } h_b}^{\text{vis, model}}$, the resulting midrapidity cross section per unit of rapidity is

$$\frac{\mathrm{d}\sigma_{b\bar{b}}}{\mathrm{d}y} = 5.52 \pm 0.77 \, (\text{stat.}) \pm 0.75 \, (\text{syst.}) \, {}^{+0.07}_{-0.12} \, (\text{extr.}) \, \text{mb}.$$

With a similar approach, the total $b\bar{b}$ production cross section is obtained by extrapolating the visible cross section to the full phase space:

$$\sigma(\mathrm{p} + \mathrm{Pb} \to b\bar{b} + X) = \alpha_{4\pi} \frac{\sigma_{J/\psi \text{ from } h_b}^{\text{vis}}}{2 \times BR(\mathrm{h}_b \to J/\psi + X)}, \tag{10}$$
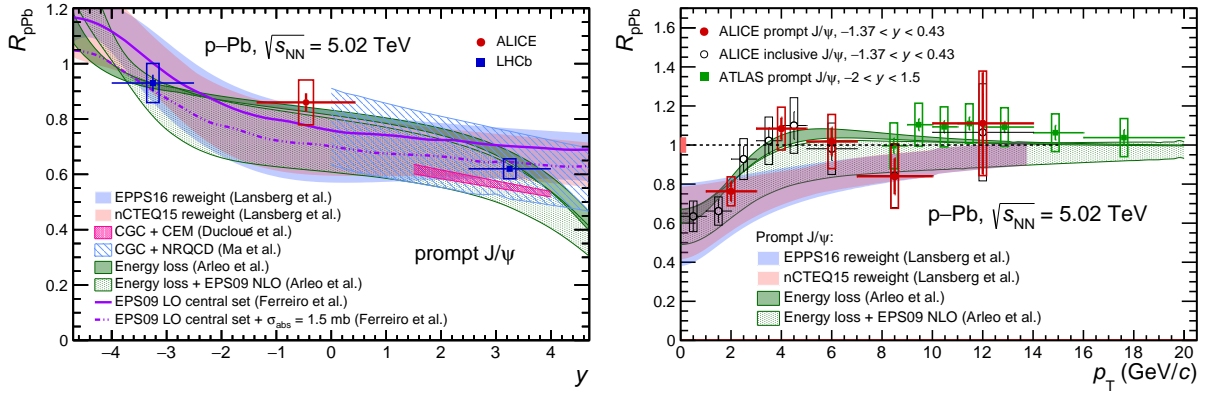
15

Figure 7: R_{pPb} of prompt J/ψ as a function of rapidity (left panel) and as a function of p_{T} along with that of inclusive J/ψ at midrapidity (right panel). Results are shown in comparison with LHCb measurements [64] at backward and forward rapidity in the left panel and with ATLAS results [14] (shown up to $p_{\text{T}} = 20$ GeV/c) in the right-hand panel. Statistical uncertainties are represented by vertical error bars, while open boxes correspond to systematic uncertainties. In the left panel, the systematic uncertainty of the ALICE data point includes also the contribution from the extrapolation procedure to go from the visible region ($p_{\text{T}} > 1$ GeV/c) to $p_{\text{T}} > 0$. The filled box around $R_{\text{pPb}} = 1$ in the right panel indicates the size of the global relative uncertainty of the ALICE measurements. The results of various model predictions for prompt J/ψ implementing different CNM effects are also shown [44, 101, 106–108].

where the factor $\alpha_{4\pi}$ is defined as the ratio of the yield of non-prompt J/ψ produced in the full phase space to that in the visible region, and the factor 2 takes into account that hadrons with b or $\bar{\text{b}}$ valence quark can decay into J/ψ. The value of the $\alpha_{4\pi}$ factor obtained from FONLL pQCD calculations with EPPS16 nPDFs, with the b-quark fragmentation performed using PYTHIA 6.4 with the Perugia-0 tune, is $\alpha_{4\pi} = 4.10 \, ^{+0.14}_{-0.12}$. Using PYTHIA 8 instead of FONLL for the generation of b$\bar{\text{b}}$ quark pairs provides
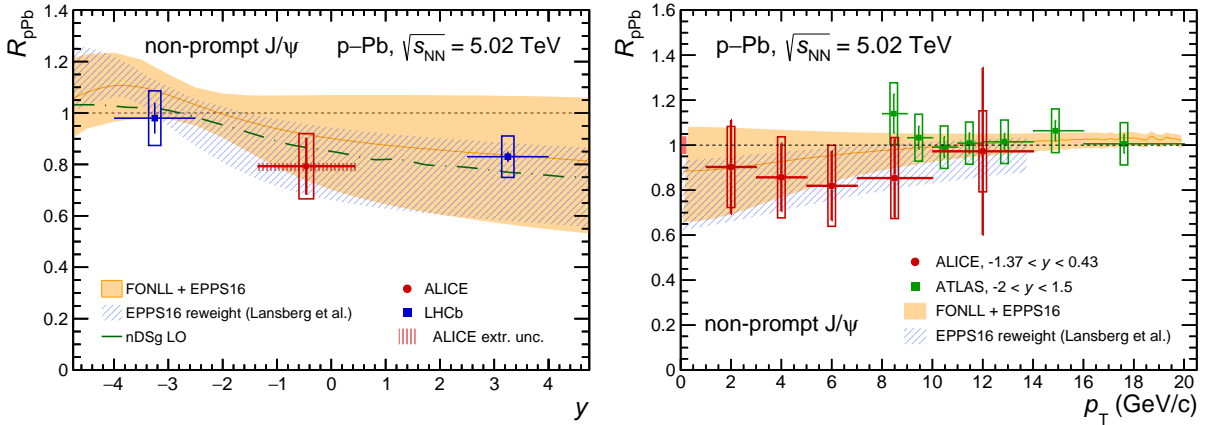
Figure 8: Nuclear modification factor R_{pPb} of non-prompt J/ψ as a function of rapidity (left panel) and as a function of p_{T} at midrapidity (right panel). The results are compared with similar measurements from the LHCb [64] and ATLAS [14] experiments. Vertical bars and the open boxes indicate the statistical and systematic uncertainties, respectively. The uncertainty due to the extrapolation to $p_{\text{T}} = 0$ GeV/c for the ALICE measurement is reported as a shaded box in left panel, while the filled box around $R_{\text{pPb}} = 1$ in the right-hand panel denotes the size of the global normalisation uncertainty. The predicted nuclear modification factors according to the nDSg [109] (central value shown in the left panel only) and EPPS16 [95] parameterisations (including a reweighted computation from [101]) are shown superimposed on both panels.

the value 4.02, which is 2% smaller than the used value for the extrapolation based on FONLL. The total cross section is[2]

$$\sigma(p + Pb \rightarrow b\bar{b} + X) = 35.5 \pm 5.0 \text{ (stat.)} \pm 4.8 \text{ (syst.)} {}^{+1.2}_{-1.0} \text{ (extr.) mb.}$$

The reported results for the extrapolated $b\bar{b}$ production cross sections are consistent with our previous derivations [51]. The total uncertainty is reduced by a factor of 2 thanks to the larger data sample, the smaller systematic uncertainty, and the slightly extended coverage of the visible region where the non-prompt J/ψ cross section is measured.

In p–Pb collisions at $\sqrt{s_{NN}} = 5.02$ TeV the LHCb Collaboration measured the non-prompt J/ψ production cross section at forward and backward rapidities for $p_T < 14$ GeV/c, reporting [64] $\sigma_{J/\psi \text{ from } h_b}(1.5 < y < 4.0) = 166.0 \pm 4.1 \pm 8.2$ μb and $\sigma_{J/\psi \text{ from } h_b}(-5.0 < y < -2.5) = 118.2 \pm 6.8 \pm 11.7$ μb, respectively. A more precise estimate of the total $b\bar{b}$ cross section can be obtained by repeating the same procedure with including also these results from the LHCb collaboration [64], to obtain a wider visible region: $(-5 < y < -2.5, p_T < 14 \text{ GeV}/c) \cup (-1.37 < y < 0.43, p_T > 1.0 \text{ GeV}/c) \cup (1.5 < y < 4, p_T < 14 \text{ GeV}/c)$. The cross section in this wider visible region is obtained as the sum of the cross sections measured in this work at central rapidity and those from LHCb. All the uncertainties are uncorrelated except that of the branching ratio. In this case, the $\alpha_{4\pi}$ factor, which is calculated as the ratio of the yield from the model in full phase space to that in the wider region covered by the ALICE and LHCb experiments, is reduced to 1.60 ± 0.02, and the corresponding total cross section is

$$\sigma(p + Pb \rightarrow b\bar{b} + X) = 33.8 \pm 2.0 \text{ (stat.)} \pm 3.4 \text{ (syst.)} {}^{+0.4}_{-0.5} \text{ (extr.) mb} \quad \text{(ALICE and LHCb).}$$

4 Summary

The production of J/ψ mesons in p−Pb collisions at $\sqrt{s_{NN}} = 5.02$ TeV is studied based on a data sample about six times larger than that of previously published results yielding smaller uncertainties and extending the p_T coverage. The inclusive J/ψ production cross section at midrapidity is measured down to $p_T = 0$ after reconstructing the J/ψ mesons in the dielectron decay channel. The fraction of the inclusive J/ψ yield originated from b-hadron decays is then determined on a statistical basis, allowing the prompt and non-prompt J/ψ production cross sections at midrapidity to be derived for $p_T > 1$ GeV/c and as a function of p_T in five momentum intervals. The results are scaled to reference measurements from pp collisions at the same centre-of-mass energy in order to investigate the presence of nuclear effects on J/ψ production. The nuclear modification factor of prompt J/ψ shows a significant suppression for $p_T \lesssim 3$ GeV/c, whereas there is a hint of a less pronounced suppression of the non-prompt component over the inspected p_T range. The results can be described by theoretical calculations including various combinations of cold nuclear matter effects, although a precise discrimination among the different models is impaired by the uncertainties affecting the currently available predictions. Finally, the measurement of the non-prompt J/ψ production cross section is used to derive the extrapolated midrapidity $d\sigma_{b\bar{b}}/dy$ and total cross section, $\sigma_{b\bar{b}}$, of beauty quark production.

Acknowledgements

---

[2]The extrapolation uncertainties for the $d\sigma_{b\bar{b}}/dy$ and for the total $b\bar{b}$ cross section include the contributions related to the FONLL, CTEQ6.6 and EPPS16 uncertainties as discussed in Ref. [51], and also a minor contribution of about 0.4% related to the uncertainty on the p_T-dependence of the relative abundance of b-hadron species.

References

[1] **D0** Collaboration, S. Abachi *et al.*, "J/ψ production in p$\bar{\mathrm{p}}$ Collisions at $\sqrt{s} = 1.8$ TeV", *Phys. Lett. B* **370** (1996) 279.

[2] **D0** Collaboration, B. Abbott *et al.*, "Small Angle J/ψ Production in p$\bar{\mathrm{p}}$ Collisions at $\sqrt{s} = 1.8$ TeV", *Phys. Rev. Lett.* **82** (1999) 35.

[3] **CDF** Collaboration, D. Acosta *et al.*, "Measurement of the J/ψ meson and b-hadron production cross sections in p$\bar{\mathrm{p}}$ collisions at $\sqrt{s} = 1960$ GeV ", *Phys. Rev. D* **71** (2005) 032001.

[4] **CDF** Collaboration, A. Abulencia *et al.*, "Polarizations of J/ψ and $\psi(2S)$ Mesons Produced in p$\bar{\mathrm{p}}$ Collisions at $\sqrt{s} = 1.96$ TeV ", *Phys. Rev. Lett.* **99** (2007) 132001.

[5] **PHENIX** Collaboration, A. Adare *et al.*, "*J*/ψ production versus transverse momentum and rapidity in $p + p$ collisions at $\sqrt{s} = 200$ GeV", *Phys. Rev. Lett.* **98** (2007) 232002, arXiv:hep-ex/0611020 [hep-ex].

[6] **STAR** Collaboration, J. Adam *et al.*, "Measurements of the transverse-momentum-dependent cross sections of *J*/ψ production at mid-rapidity in proton+proton collisions at $\sqrt{s} = 510$ and 500 GeV with the STAR detector", *Phys. Rev.* **D100** (2019) 052009, arXiv:1905.06075 [hep-ex].

[7] **ALICE** Collaboration, S. Acharya *et al.*, "Inclusive J/ψ production at mid-rapidity in pp collisions at $\sqrt{s} = 5.02$ TeV", *J. High Energ. Phys.* **10** (2019) 084, arXiv:1905.07211 [nucl-ex].

[8] **ALICE** Collaboration, B. Abelev *et al.*, "Inclusive *J*/ψ production in *pp* collisions at $\sqrt{s} = 2.76$ TeV", *Phys. Lett. B* **718** (2012) 295–306, arXiv:1203.3641 [hep-ex]. [Erratum: Phys.Lett.B 748, 472–473 (2015)].

[9] **ALICE** Collaboration, K. Aamodt *et al.*, "Rapidity and transverse momentum dependence of inclusive J/ψ production in *pp* collisions at $\sqrt{s} = 7$ TeV", *Phys. Lett. B* **704** (2011) 442–455, arXiv:1105.0380 [hep-ex]. [Erratum: Phys.Lett.B 718, 692–698 (2012)].

[10] **ALICE** Collaboration, J. Adam *et al.*, "J/ψ suppression at forward rapidity in Pb-Pb collisions at $\sqrt{s_{\mathrm{NN}}} = 5.02$ TeV", *Phys. Lett. B* **766** (2017) 212–224, arXiv:1606.08197 [nucl-ex].

[11] **ALICE** Collaboration, J. Adam *et al.*, "Inclusive quarkonium production at forward rapidity in pp collisions at $\sqrt{s} = 8$ TeV", *Eur. Phys. J. C* **76** (2016) 184, arXiv:1509.08258 [hep-ex].

[12] **ALICE** Collaboration, S. Acharya *et al.*, "Energy dependence of forward-rapidity J/ψ and $\psi(2S)$ production in pp collisions at the LHC", *Eur. Phys. J. C* **77** (2017) 392, arXiv:1702.00557 [hep-ex].

[13] **ALICE** Collaboration, B. Abelev *et al.*, "Measurement of prompt *J*/ψ and beauty hadron production cross sections at mid-rapidity in pp collisions at $\sqrt{s} = 7$ TeV", *J. High Energ. Phys.* **11** (2012) 065, arXiv:1205.5880 [hep-ex].

[14] **ATLAS** Collaboration, M. Aaboud *et al.*, "Measurement of quarkonium production in proton–lead and proton–proton collisions at 5.02 TeV with the ATLAS detector", *Eur. Phys. J. C78* (2018) 171, arXiv:1709.03089 [nucl-ex].

[15] **CMS** Collaboration, A. M. Sirunyan *et al.*, "Measurement of prompt and nonprompt J/ψ production in pp and pPb collisions at $\sqrt{s_{\mathrm{NN}}} = 5.02$ TeV", *Eur. Phys. J. C77* (2017) 269, arXiv:1702.01462 [nucl-ex].

[16] **LHCb** Collaboration, R. Aaij *et al.*, "Measurement of J/ψ production in *pp* collisions at $\sqrt{s} = 2.76$ TeV", *J. High Energ. Phys.* **02** (2013) 041, `arXiv:1212.1045 [hep-ex]`.

[17] **LHCb** Collaboration, R. Aaij *et al.*, "Measurement of J/ψ production in *pp* collisions at $\sqrt{s} = 7$ TeV", *Eur. Phys. J.* **C71** (2011) 1645, `arXiv:1103.0423 [hep-ex]`.

[18] **LHCb** Collaboration, R. Aaij *et al.*, "Production of J/ψ and Υ mesons in *pp* collisions at $\sqrt{s} = 8$ TeV", *J. High Energ. Phys.* **06** (2013) 064, `arXiv:1304.6977 [hep-ex]`.

[19] **LHCb** Collaboration, R. Aaij *et al.*, "Measurement of forward J/ψ production cross-sections in *pp* collisions at $\sqrt{s} = 13$ TeV", *J. High Energ. Phys.* **10** (2015) 172, `arXiv:1509.00771 [hep-ex]`. [Erratum: J. High Energ. Phys. 05, 063 (2017)].

[20] G. T. Bodwin, E. Braaten, and G. P. Lepage, "Rigorous QCD analysis of inclusive annihilation and production of heavy quarkonium", *Phys. Rev. D* **51** (1995) 1125, `arXiv:hep-ph/9407339 [hep-ph]`.

[21] P. Cho and A. Leibovich, "Color-octet quarkonia production", *Phys. Rev. D* **53** (1996) 150.

[22] P. Cho and A. Leibovich, "Color-octet quarkonia production II", *Phys. Rev. D* **53** (1996) 6203.

[23] N. Brambilla *et al.*, "Heavy quarkonium: progress, puzzles, and opportunities", *Eur. Phys. J. C* **71** (2011) 1534, `arXiv:1010.5827 [hep-ph]`.

[24] A. Andronic *et al.*, "Heavy-flavour and quarkonium production in the LHC era: from proton-proton to heavy-ion collisions", *Eur. Phys. J. C* **76** (2016) 107, `arXiv:1506.03981 [nucl-ex]`.

[25] M. Butenschoen and B. A. Kniehl, "NEXT-TO-LEADING ORDER TESTS OF NON-RELATIVISTIC-QCD FACTORIZATION WITH J/ψ YIELD AND POLARIZATION", *Mod. Phys. Lett. A* **28** (2013) 1350027, `arXiv:1212.2037 [hep-ph]`.

[26] H. Han, Y.-Q. Yan-Qing Ma, C. Meng, H.-S. Shao, and K.-T. Chao, "η_c production at lhc and implications for the understanding of j/ψ production", *Phys. Rev. Lett.* **114** (2015) 092005, `arXiv:1411.7350 [hep-ph]`.

[27] H.-F. Zhang, Z. Sun, W.-L. Sang, and R. Li, "Impact of η_c hadroproduction data on charmonium production and polarization within the nonrelativistic qcd framework", *Phys. Rev. Lett.* **114** (2015) 092006, `arXiv:1412.0508 [hep-ph]`.

[28] M. Butenschoen, Z.-G. He, and B. A. Kniehl, "η_c production at the lhc challenges nonrelativistic qcd factorization", *Phys. Rev. Lett.* **114** (2015) 092004, `arXiv:1411.5287 [hep-ph]`.

[29] G. Aarts *et al.*, "Heavy-flavor production and medium properties in high-energy nuclear collisions — What next?", *Eur. Phys. J. A* **53** (2017) 93, `arXiv::1612.08032 [nucl-th]`.

[30] **European Muon** Collaboration, "The ratio of the nucleon structure functions f_n^2 for iron and deuterium", *Phys. Lett. B* **123** (1983) 275.

[31] A. Kusina *et al.*, "nCTEQ15 - Global analysis of nuclear parton distributions with uncertainties", *PoS* **DIS2015** (2015) 041, `arXiv:1509.01801 [hep-ph]`.

[32] K. J. Eskola, P. Paakkinen, H. Paukkunen, and C. A. Salgado, "EPPS16: Nuclear parton distributions with LHC data", *Eur. Phys. J. C* **77** (2017) 163, `arXiv:1612.05741 [hep-ph]`.

[33] R. Abdul Khalek, J. J. Ethier, J. Rojo, and G. van Weelden, "nNNPDF2.0: quark flavor separation in nuclei from LHC data", *JHEP* **09** (2020) 183, `arXiv:2006.14629 [hep-ph]`.

[34] K. J. Eskola, I. Helenius, P. Paakkinen, and H. Paukkunen, "A QCD analysis of LHCb D-meson data in p+Pb collisions", *JHEP* **05** (2020) 037, `arXiv:1906.02512 [hep-ph]`.

[35] K. J. Eskola, I. Helenius, P. Paakkinen, and H. Paukkunen, "Impact of dijet and D-meson data from 5.02 TeV p+Pb collisions on nuclear PDFs", *Nucl. Phys. A* **1005** (2021) 121944, `arXiv:2001.10385 [hep-ph]`.

[36] A. Kusina, J.-P. Lansberg, I. Schienbein, and H.-S. Shao, "Reweighted nuclear PDFs using Heavy-Flavor Production Data at the LHC: nCTEQ15_rwHF & EPPS16_rwHF", *Phys. Rev. D* **104** (2021) 014010, `arXiv:2012.11462 [hep-ph]`.

[37] J.-P. Blaizot, F. Gelis, and R. Venugopalan, "High energy pA collisions in the color glass condensate approach II: quark pair production", *Nucl. Phys. A* **743** (2004) 57, `hep-ph/0402257`.

[38] F. Gelis, "Color Glass Condensate and Glasma", *Int. J. Mod. Phys. A* **28** (2013) 1330001, `arXiv:1211.3327 [hep-ph]`.

[39] H. Fujii and K. Watanabe, "Heavy quark pair production in high energy pA collisions: Open heavy flavors", *Nucl. Phys. A* **920** (2013) 78–93, `arXiv:1308.1258 [hep-ph]`.

[40] I. Vitev, "Non-Abelian energy loss in cold nuclear matter", *Phys. Rev. C* **75** (2007) 064906, `hep-th/0703002`.

[41] M. Lev and B. Petersson, "Nuclear effects at large transverse momentum in a QCD parton model", *Z. Phys. C* **21** (1983) 155.

[42] X. Wang, "Systematic study of high p_{T} hadron spectra in pp, pA, and AA collisions at ultrarelativistic energies", *Phys. Rev. C* **61** (2000) 064910, `nucl-th/9812021`.

[43] B. Kopeliovich, J. Nemchik, A. Schäfer, and A. Tarasov, "Cronin Effect in Hadron Production Off Nuclei", *Phys. Rev. Lett.* **88** (2002) 232303, `hep-ph/0201010`.

[44] F. Arleo, R. Kolevatov, S. Peigné, and M. Rustamova, "Centrality and $p_\perp$ dependence of J/ψ suppression in proton-nucleus collisions from parton energy loss", *J. High Energ. Phys.* **05** (2013) 155, `arXiv:1304.0901 [hep-ph]`.

[45] C. Gerschel and H. J., "A Contribution to the Suppression of the J/ψ Meson Produced in High-Energy Nucleus Nucleus Collisions", *Phys. Lett. B* **207** (1988) 253–256, `hep-ph/0201010`.

[46] **NA50** Collaboration, B. Alessandro *et al.*, "Charmonia and Drell-Yan production in proton-nucleus collisions at the CERN SPS", *Phys. Lett. B* **553** (2003) 167–178.

[47] **PHENIX** Collaboration, A. Adare *et al.*, "Transverse-Momentum Dependence of the J/ψ Nuclear Modification in d+Au Collisions at $\sqrt{s_{\mathrm{NN}}} = 200$ GeV ", *Phys. Rev. C* **87** (2013) 034904, `arXiv:1204.0777 [nucl-ex]`.

[48] J. Hufner, Y. Ivanov, B. Kopeliovich, and A. Tarasov, "Photoproduction of charmonia and total charmonium proton cross-sections", *Phys. Rev. D* **62** (2000) 094022, `hep-ph/0007111`.

[49] D. Kharzeev and R. L. Thews, "Quarkonium formation time in a model independent approach", *Phys. Rev. C* **60** (1999) 041901, `nucl-th/9907021`.

[50] **ALICE** Collaboration, J. Adam *et al.*, "Centrality dependence of $\psi(2S)$ suppression in p-Pb collisions at $\sqrt{s_{\mathrm{NN}}} = 5.02$ TeV", *J. High Energ. Phys.* **06** (2016) 050, `arXiv:1603.02816 [nucl-ex]`.

[51] **ALICE** Collaboration, S. Acharya *et al.*, "Prompt and non-prompt J/ψ production and nuclear modification at mid-rapidity in p–Pb collisions at $\sqrt{s_{\mathrm{NN}}} = \mathbf{5.02}$ TeV", *Eur. Phys. J.* **C78** (2018) 466, `arXiv:1802.00765` `[nucl-ex]`.

[52] J. C. Collins, D. E. Soper, and G. F. Sterman, "Factorization of Hard Processes in QCD", *Adv. Ser. Direct. High Energy Phys.* **5** (1989) 1–91, `hep-ph/0409313`.

[53] S. Catani, M. Ciafaloni, and F. Hautmann, "High-energy factorization and small x heavy flavor production", *Nucl. Phys. B* **336** (1991) 135–188.

[54] F. Arleo, S. Peigne, and T. Sami, "Revisiting scaling properties of medium-induced gluon radiation", *Phys. Rev. D* **83** (2011) 114036, `arXiv:1006.0818` `[hep-ph]`.

[55] **ALICE** Collaboration, B. Abelev *et al.*, "J/ψ production and nuclear effects in p-Pb collisions at $\sqrt{s_{\mathrm{NN}}} = 5.02$ TeV", *J. High Energ. Phys.* **2014** (2014) 73, `arXiv:1308.6726` `[nucl-ex]`.

[56] **ALICE** Collaboration, J. Adam *et al.*, "Centrality dependence of inclusive J/ψ production in p-Pb collisions at $\sqrt{s_{\mathrm{NN}}} = 5.02$ TeV", *J. High Energ. Phys.* **11** (2015) 127, `arXiv:1506.08808` `[nucl-ex]`.

[57] **ALICE** Collaboration, J. Adam *et al.*, "Rapidity and transverse-momentum dependence of the inclusive J/ψ nuclear modification factor in p-Pb collisions at $\sqrt{s_{NN}} = 5.02$ TeV", *J. High Energ. Phys.* **06** (2015) 055, `arXiv:1503.07179` `[nucl-ex]`.

[58] **ALICE** Collaboration, S. Acharya *et al.*, "Inclusive J/ψ production at forward and backward rapidity in p-Pb collisions at $\sqrt{s_{\mathrm{NN}}} = 8.16$ TeV", *J. High Energ. Phys.* **07** (2018) 160, `arXiv:1805.04381` `[nucl-ex]`.

[59] **ALICE** Collaboration, J. Adam *et al.*, "Measurement of electrons from beauty-hadron decays in p-Pb collisions at $\sqrt{s_{\mathrm{NN}}} = 5.02$ TeV and Pb-Pb collisions at $\sqrt{s_{\mathrm{NN}}} = 2.76$ TeV", *J. High Energ. Phys.* **07** (2017) 052, `arXiv:1609.03898` `[nucl-ex]`.

[60] **ATLAS** Collaboration, G. Aad *et al.*, "Measurement of differential J/ψ production cross sections and forward-backward ratios in p + Pb collisions with the ATLAS detector", *Phys. Rev.* **C92** (2015) 034904, `arXiv:1505.08141` `[hep-ex]`.

[61] **CMS** Collaboration, V. Khachatryan *et al.*, "Transverse momentum spectra of inclusive b jets in pPb collisions at $\sqrt{s_{NN}} = 5.02$ TeV", *Phys. Lett.* **B754** (2016) 59, `arXiv:1510.03373` `[nucl-ex]`.

[62] **CMS** Collaboration, V. Khachatryan *et al.*, "Study of B Meson Production in p+Pb Collisions at $\sqrt{s_{NN}} = 5.02$ TeV Using Exclusive Hadronic Decays", *Phys. Rev. Lett.* **116** (2016) 032301, `arXiv:1508.06678` `[nucl-ex]`.

[63] **CMS** Collaboration, A. M. Sirunyan *et al.*, "Measurement of prompt $\psi(2S)$ production cross sections in proton-lead and proton-proton collisions at $\sqrt{s_{\mathrm{NN}}} = 5.02$ TeV", *Phys. Lett.* **B790** (2019) 509–532, `arXiv:1805.02248` `[hep-ex]`.

[64] **LHCb** Collaboration, R. Aaij *et al.*, "Study of J/ψ production and cold nuclear matter effects in pPb collisions at $\sqrt{s_{NN}} = 5$ TeV", *J. High Energ. Phys.* **02** (2014) 072, `arXiv:1308.6729` `[nucl-ex]`.

[65] **LHCb** Collaboration, R. Aaij *et al.*, "Study of $\psi(2S)$ production and cold nuclear matter effects in pPb collisions at $\sqrt{s_{NN}} = 5$ TeV", *J. High Energ. Phys.* **03** (2016) 133, `arXiv:1601.07878` `[nucl-ex]`.

[66] **LHCb** Collaboration, R. Aaij *et al.*, "Prompt and nonprompt J/ψ production and nuclear modification in *p*Pb collisions at $\sqrt{s_{NN}}$ = 8.16 TeV", *Phys. Lett.* **B774** (2017) 159–178, `arXiv:1706.07122 [hep-ex]`.

[67] **LHCb** Collaboration, R. Aaij *et al.*, "Measurement of B^+, B^0 and Λ_b^0 production in *p*Pb collisions at $\sqrt{s_{NN}}$ = 8.16 TeV", *Phys. Rev. D* **99** (2019) 052011, `arXiv:1902.05599 [hep-ex]`.

[68] **ALICE** Collaboration, D. Adamová *et al.*, "J/ψ production as a function of charged-particle pseudorapidity density in p-Pb collisions at $\sqrt{s_{NN}}$ = 5.02 TeV", *Phys. Lett. B* **776** (2018) 91–104, `arXiv:1704.00274 [nucl-ex]`.

[69] **ALICE** Collaboration, K. Aamodt *et al.*, "The ALICE experiment at the CERN LHC", *JINST* **3** (2008) S08002.

[70] **ALICE** Collaboration, B. Abelev *et al.*, "Performance of the ALICE Experiment at the CERN LHC", *Int. J. Mod. Phys.* **A29** (2014) 1430044, `arXiv:1402.4476 [nucl-ex]`.

[71] **ALICE** Collaboration, K. Aamodt *et al.*, "Alignment of the ALICE Inner Tracking System with cosmic-ray tracks", *JINST* **5** (2010) P03003, `arXiv:1001.0502 [physics.ins-det]`.

[72] J. Alme *et al.*, "The ALICE TPC, a large 3-dimensional tracking device with fast readout for ultra-high multiplicity events", *Nucl. Instrum. Meth.* **A622** (2010) 316–367, `arXiv:1001.1950 [physics.ins-det]`.

[73] **ALICE** Collaboration, B. Abelev *et al.*, "Measurement of visible cross sections in proton-lead collisions at $\sqrt{s_{NN}}$ = 5.02 TeV in van der Meer scans with the ALICE detector", *JINST* **9** (2014) P11003, `arXiv:1405.1849 [nucl-ex]`.

[74] **ALICE** Collaboration, E. Abbas *et al.*, "Performance of the ALICE VZERO system", *JINST* **8** (2013) P10016, `arXiv:1306.3130 [nucl-ex]`.

[75] **ALICE** Collaboration, B. Abelev *et al.*, "Pseudorapidity density of charged particles in p + Pb collisions at $\sqrt{s_{NN}}$ = 5.02 TeV", *Phys. Rev. Lett.* **110** (2013) 032301, `arXiv:1210.3615 [nucl-ex]`.

[76] R. Brun, F. Bruyant, F. Carminati, S. Giani, M. Maire, A. McPherson, G. Patrick, and L. Urban, "GEANT Detector Description and Simulation Tool", CERN-W5013, CERN-W-5013, W5013, W-5013. `http://cds.cern.ch/record/1082634`.

[77] J. Gaiser *et al.*, "Charmonium Spectroscopy from Inclusive ψ′ and J/ψ Radiative Decays", *Phys. Rev.* **D34** (1986) 711.

[78] T. Pierog, I. Karpenko, J. M. Katzy, E. Yatsenko, and K. Werner, "EPOS LHC: Test of collective hadronization with data measured at the CERN Large Hadron Collider", *Phys. Rev.* **C92** (2015) 034906, `arXiv:1306.0121 [hep-ph]`.

[79] H. Fritzsch, "Producing Heavy Quark Flavors in Hadronic Collisions: A Test of Quantum Chromodynamics", *Phys. Lett.* **67B** (1977) 217–221.

[80] J. L. Albacete *et al.*, "Predictions for p–Pb Collisions at $\sqrt{s_{NN}}$ = 5 TeV", *Int. J. Mod. Phys.* **E22** (2013) 1330007, `arXiv:1301.3395 [hep-ph]`.

[81] K. J. Eskola, H. Paukkunen, and C. A. Salgado, "EPS09: A New Generation of NLO and LO Nuclear Parton Distribution Functions", *J. High Energ. Phys.* **04** (2009) 065, `arXiv:0902.4154 [hep-ph]`.

[82] D. J. Lange, "The EvtGen particle decay simulation package", *Nucl. Instrum. Meth.* **A462** (2001) 152–155.

[83] E. Barberio and Z. Was, "PHOTOS: A Universal Monte Carlo for QED radiative corrections. Version 2.0", *Comput. Phys. Commun.* **79** (1994) 291–308.

[84] **Particle Data Group** Collaboration, M. Tanabashi *et al.*, "Review of Particle Physics", *Phys. Rev.* **D98** (2018) 030001.

[85] **ALICE** Collaboration, S. Acharya *et al.*, "Measurement of D-meson production at mid-rapidity in pp collisions at $\sqrt{s} = 7$ TeV", *Eur. Phys. J. C* **77** (2017) 550, `arXiv:1702.00766 [hep-ex]`.

[86] F. Bossu, Z. C. del Valle, A. de Falco, M. Gagliardi, S. Grigoryan, and G. Martinez Garcia, "Phenomenological interpolation of the inclusive J/psi cross section to proton-proton collisions at 2.76 TeV and 5.5 TeV", `arXiv:1103.2394 [nucl-ex]`.

[87] **ALICE** Collaboration, J. Adam *et al.*, "Inclusive, prompt and non-prompt J/ψ production at mid-rapidity in Pb-Pb collisions at $\sqrt{s_{NN}}$ = 2.76 TeV", *J. High Energ. Phys.* **07** (2015) 051, `arXiv:1504.07151 [nucl-ex]`.

[88] T. Sjostrand, S. Mrenna, and P. Z. Skands, "PYTHIA 6.4 Physics and Manual", *J. High Energ. Phys.* **05** (2006) 026, `arXiv:hep-ph/0603175 [hep-ph]`.

[89] P. Z. Skands, "Tuning Monte Carlo Generators: The Perugia Tunes", *Phys. Rev.* **D82** (2010) 074018, `arXiv:1005.3457 [hep-ph]`.

[90] M. Cacciari, S. Frixione, N. Houdeau, M. L. Mangano, P. Nason, and G. Ridolfi, "Theoretical predictions for charm and bottom production at the LHC", *J. High Energ. Phys.* **10** (2012) 137, `arXiv:1205.6344 [hep-ph]`.

[91] **LHCb** Collaboration, R. Aaij *et al.*, "Measurement of b hadron fractions in 13 TeV pp collisions", *Phys. Rev. D* **100** (2019) 031102, `arXiv:1902.06794 [hep-ex]`.

[92] **ALICE** Collaboration, B. Abelev *et al.*, "J/ψ polarization in pp collisions at $\sqrt{s} = 7$ TeV", *Phys. Rev. Lett.* **108** (2012) 082001, `arXiv:1111.1630 [hep-ex]`.

[93] **CMS** Collaboration, S. Chatrchyan *et al.*, "Measurement of the Prompt J/ψ and $\psi(2S)$ Polarizations in pp Collisions at $\sqrt{s} = 7$ TeV", *Phys. Lett.* **B727** (2013) 381–402, `arXiv:1307.6070 [hep-ex]`.

[94] **ALICE** Collaboration, S. Acharya *et al.*, "Measurement of the inclusive J/ψ polarization at forward rapidity in pp collisions at $\sqrt{s} = 8$ TeV", *Eur. Phys. J. C* **78** (2018) 562, `arXiv:1805.04374 [hep-ex]`.

[95] K. J. Eskola, P. Paakkinen, H. Paukkunen, and C. A. Salgado, "EPPS16: Nuclear parton distributions with LHC data", *Eur. Phys. J. C* **77** (2017) 163, `arXiv:1612.05741 [hep-ph]`.

[96] **ATLAS** Collaboration, G. Aad *et al.*, "Measurement of the differential cross-sections of inclusive, prompt and non-prompt J/ψ production in proton-proton collisions at $\sqrt{s} = 7$ TeV", *Nucl. Phys.* **B850** (2011) 387–444, `arXiv:1104.3038 [hep-ex]`.

[97] **CMS** Collaboration, V. Khachatryan *et al.*, "Prompt and Non-Prompt J/ψ Production in pp Collisions at $\sqrt{s} = 7$ TeV", *Eur. Phys. J. C* **71** (2011) 1575, `arXiv:1011.4193 [hep-ex]`.

[98] **ATLAS** Collaboration, G. Aad *et al.*, "Measurement of the differential cross-sections of prompt and non-prompt production of J/ψ and $\psi(2S)$ in pp collisions at $\sqrt{s} = 7$ and 8 TeV with the ATLAS detector", *Eur. Phys. J. C* **76** (2016) 283, `arXiv:1512.03657 [hep-ex]`.

[99] P. M. Nadolsky, H.-L. Lai, Q.-H. Cao, J. Huston, J. Pumplin, D. Stump, W.-K. Tung, and C.-P. Yuan, "Implications of CTEQ global analysis for collider observables", *Phys. Rev. D* **78** (2008) 013004, arXiv:0802.0007 [hep-ph].

[100] J.-P. Lansberg and H.-S. Shao, "Towards an automated tool to evaluate the impact of the nuclear modification of the gluon density on quarkonium, D and B meson production in proton–nucleus collisions", *Eur. Phys. J.* **C77** (2017) 1, arXiv:1610.05382 [hep-ph].

[101] A. Kusina, J.-P. Lansberg, I. Schienbein, and H.-S. Shao, "Gluon Shadowing in Heavy-Flavor Production at the LHC", *Phys. Rev. Lett.* **121** (2018) 052004, arXiv:1712.07024 [hep-ph].

[102] H.-S. Shao, "HELAC-Onia: An automatic matrix element generator for heavy quarkonium physics", *Comput. Phys. Commun.* **184** (2013) 2562–2570, arXiv:1212.5293 [hep-ph].

[103] H.-S. Shao, "HELAC-Onia 2.0: an upgraded matrix-element and event generator for heavy quarkonium physics", *Comput. Phys. Commun.* **198** (2016) 238–259, arXiv:1507.03435 [hep-ph].

[104] K. Kovarik *et al.*, "nCTEQ15 - Global analysis of nuclear parton distributions with uncertainties in the CTEQ framework", *Phys. Rev. D* **93** (2016) 085037, arXiv:1509.00792 [hep-ph].

[105] **LHCb** Collaboration, R. Aaij *et al.*, "Study of prompt D^0 meson production in pPb collisions at $\sqrt{s_{\mathrm{NN}}} = 5$ TeV", *JHEP* **10** (2017) 090, arXiv:1707.02750 [hep-ex].

[106] E. G. Ferreiro, F. Fleuret, J. P. Lansberg, and A. Rakotozafindrabe, "Impact of the Nuclear Modification of the Gluon Densities on J/ψ production in pPb collisions at $\sqrt{s_{NN}} = 5$ TeV", *Phys. Rev. C* **88** (2013) 047901, arXiv:1305.4569 [hep-ph].

[107] B. Ducloué, T. Lappi, and H. Mäntysaari, "Forward J/ψ production in proton-nucleus collisions at high energy", *Phys. Rev. D* **91** (2015) 114005, arXiv:1503.02789 [hep-ph].

[108] Y.-Q. Ma, R. Venugopalan, and H.-F. Zhang, "J/ψ production and suppression in high energy proton-nucleus collisions", *Phys. Rev. D* **92** (2015) 071901, arXiv:1503.07772 [hep-ph].

[109] D. de Florian, R. Sassot, P. Zurita, and M. Stratmann, "Global Analysis of Nuclear Parton Distributions", *Phys. Rev. D* **85** (2012) 074028, arXiv:1112.6324 [hep-ph].

[110] **ALEPH** Collaboration, D. Buskulic *et al.*, "Measurements of mean lifetime and branching fractions of b hadrons decaying to J/ψ", *Phys. Lett. B* **295** (1992) 396–408.

[111] **L3** Collaboration, O. Adriani *et al.*, "χ_{C} production in hadronic Z decays", *Phys. Lett. B* **317** (1993) 467–473.

[112] **DELPHI** Collaboration, P. Abreu *et al.*, "J/ψ production in the hadronic decays of the Z", *Phys. Lett. B* **341** (1994) 109–122.

A   The ALICE Collaboration

S. Acharya[143], D. Adamová[98], A. Adler[76], J. Adolfsson[83], G. Aglieri Rinella[35], M. Agnello[31], N. Agrawal[55], Z. Ahammed[143], S. Ahmad[16], S.U. Ahn[78], I. Ahuja[39], Z. Akbar[52], A. Akindinov[95], M. Al-Turany[110], S.N. Alam[41], D. Aleksandrov[91], B. Alessandro[61], H.M. Alfanda[7], R. Alfaro Molina[73], B. Ali[16], Y. Ali[14], A. Alici[26], N. Alizadehvandchali[127], A. Alkin[35], J. Alme[21], T. Alt[70], L. Altenkamper[21], I. Altsybeev[115], M.N. Anaam[7], C. Andrei[49], D. Andreou[93], A. Andronic[146], M. Angeletti[35], V. Anguelov[107], F. Antinori[58], P. Antonioli[55], C. Anuj[16], N. Apadula[82], L. Aphecetche[117], H. Appelshäuser[70], S. Arcelli[26], R. Arnaldi[61], I.C. Arsene[20], M. Arslandok[148,107], A. Augustinus[35], R. Averbeck[110], S. Aziz[80], M.D. Azmi[16], A. Badalà[57], Y.W. Baek[42], X. Bai[131,110], R. Bailhache[70], Y. Bailung[51], R. Bala[104], A. Balbino[31], A. Baldisseri[140], B. Balis[2], M. Ball[44], D. Banerjee[4], R. Barbera[27], L. Barioglio[108,25], M. Barlou[87], G.G. Barnaföldi[147], L.S. Barnby[97], V. Barret[137], C. Bartels[130], K. Barth[35], E. Bartsch[70], F. Baruffaldi[28], N. Bastid[137], S. Basu[83], G. Batigne[117], B. Batyunya[77], D. Bauri[50], J.L. Bazo Alba[114], I.G. Bearden[92], C. Beattie[148], I. Belikov[139], A.D.C. Bell Hechavarria[146], F. Bellini[26,35], R. Bellwied[127], S. Belokurova[115], V. Belyaev[96], G. Bencedi[71], S. Beole[25], A. Bercuci[49], Y. Berdnikov[101], A. Berdnikova[107], D. Berenyi[147], L. Bergmann[107], M.G. Besoiu[69], L. Betev[35], P.P. Bhaduri[143], A. Bhasin[104], I.R. Bhat[104], M.A. Bhat[4], B. Bhattacharjee[43], P. Bhattacharya[23], L. Bianchi[25], N. Bianchi[53], J. Bielčík[38], J. Bielčíková[98], J. Biernat[120], A. Bilandzic[108], G. Biro[147], S. Biswas[4], J.T. Blair[121], D. Blau[91], M.B. Blidaru[110], C. Blume[70], G. Boca[29,59], F. Bock[99], A. Bogdanov[96], S. Boi[23], J. Bok[63], L. Boldizsár[147], A. Bolozdynya[96], M. Bombara[39], P.M. Bond[35], G. Bonomi[142,59], H. Borel[140], A. Borissov[84], H. Bossi[148], E. Botta[25], L. Bratrud[70], P. Braun-Munzinger[110], M. Bregant[123], M. Broz[38], G.E. Bruno[109,34], M.D. Buckland[130], D. Budnikov[111], H. Buesching[70], S. Bufalino[31], O. Bugnon[117], P. Buhler[116], Z. Buthelezi[74,134], J.B. Butt[14], S.A. Bysiak[120], D. Caffarri[93], M. Cai[28,7], H. Caines[148], A. Caliva[110], E. Calvo Villar[114], J.M.M. Camacho[122], R.S. Camacho[46], P. Camerini[24], F.D.M. Canedo[123], F. Carnesecchi[35,26], R. Caron[140], J. Castillo Castellanos[140], E.A.R. Casula[23], F. Catalano[31], C. Ceballos Sanchez[77], P. Chakraborty[50], S. Chandra[143], S. Chapeland[35], M. Chartier[130], S. Chattopadhyay[143], S. Chattopadhyay[112], A. Chauvin[23], T.G. Chavez[46], C. Cheshkov[138], B. Cheynis[138], V. Chibante Barroso[35], D.D. Chinellato[124], S. Cho[63], P. Chochula[35], P. Christakoglou[93], C.H. Christensen[92], P. Christiansen[83], T. Chujo[136], C. Cicalo[56], L. Cifarelli[26], F. Cindolo[55], M.R. Ciupek[110], G. Clai[II,55], J. Cleymans[I,126], F. Colamaria[54], J.S. Colburn[113], D. Colella[109,54,34,147], A. Collu[82], M. Colocci[35,26], M. Concas[III,61], G. Conesa Balbastre[81], Z. Conesa del Valle[80], G. Contin[24], J.G. Contreras[38], M.L. Coquet[140], T.M. Cormier[99], P. Cortese[32], M.R. Cosentino[125], F. Costa[35], S. Costanza[29,59], P. Crochet[137], E. Cuautle[71], P. Cui[7], L. Cunqueiro[99], A. Dainese[58], F.P.A. Damas[117,140], M.C. Danisch[107], A. Danu[69], I. Das[112], P. Das[89], P. Das[4], S. Das[4], S. Dash[50], S. De[89], A. De Caro[30], G. de Cataldo[54], L. De Cilladi[25], J. de Cuveland[40], A. De Falco[23], D. De Gruttola[30], N. De Marco[61], C. De Martin[24], S. De Pasquale[30], S. Deb[51], H.F. Degenhardt[123], K.R. Deja[144], L. Dello Stritto[30], S. Delsanto[25], W. Deng[7], P. Dhankher[19], D. Di Bari[34], A. Di Mauro[35], R.A. Diaz[8], T. Dietel[126], Y. Ding[138,7], R. Divià[35], D.U. Dixit[19], Ø. Djuvsland[21], U. Dmitrieva[65], J. Do[63], A. Dobrin[69], B. Dönigus[70], O. Dordic[20], A.K. Dubey[143], A. Dubla[110,93], S. Dudi[103], M. Dukhishyam[89], P. Dupieux[137], N. Dzalaiova[13], T.M. Eder[146], R.J. Ehlers[99], V.N. Eikeland[21], D. Elia[54], B. Erazmus[117], F. Ercolessi[26], F. Erhardt[102], A. Erokhin[115], M.R. Ersdal[21], B. Espagnon[80], G. Eulisse[35], D. Evans[113], S. Evdokimov[94], L. Fabbietti[108], M. Faggin[28], J. Faivre[81], F. Fan[7], A. Fantoni[53], M. Fasel[99], P. Fecchio[31], A. Feliciello[61], G. Feofilov[115], A. Fernández Téllez[46], A. Ferrero[140], A. Ferretti[25], V.J.G. Feuillard[107], J. Figiel[120], S. Filchagin[111], D. Finogeev[65], F.M. Fionda[56,21], G. Fiorenza[35,109], F. Flor[127], A.N. Flores[121], S. Foertsch[74], P. Foka[110], S. Fokin[91], E. Fragiacomo[62], E. Frajna[147], U. Fuchs[35], N. Funicello[30], C. Furget[81], A. Furs[65], J.J. Gaardhøje[92], M. Gagliardi[25], A.M. Gago[114], A. Gal[139], C.D. Galvan[122], P. Ganoti[87], C. Garabatos[110], J.R.A. Garcia[46], E. Garcia-Solis[10], K. Garg[117], C. Gargiulo[35], A. Garibli[90], K. Garner[146], P. Gasik[110], E.F. Gauger[121], A. Gautam[129], M.B. Gay Ducati[72], M. Germain[117], J. Ghosh[112], P. Ghosh[143], S.K. Ghosh[4], M. Giacalone[26], P. Gianotti[53], P. Giubellino[110,61], P. Giubilato[28], A.M.C. Glaenzer[140], P. Glässel[107], D.J.Q. Goh[85], V. Gonzalez[145], L.H. González-Trueba[73], S. Gorbunov[40], M. Gorgon[2], L. Görlich[120], S. Gotovac[36], V. Grabski[73], L.K. Graczykowski[144], L. Greiner[82], A. Grelli[64], C. Grigoras[35], V. Grigoriev[96], A. Grigoryan[I,1], S. Grigoryan[77,1], O.S. Groettvik[21], F. Grosa[35,61], J.F. Grosse-Oetringhaus[35], R. Grosso[110], G.G. Guardiano[124], R. Guernane[81], M. Guilbaud[117], K. Gulbrandsen[92], T. Gunji[135], A. Gupta[104], R. Gupta[104], I.B. Guzman[46], S.P. Guzman[46], L. Gyulai[147], M.K. Habib[110], C. Hadjidakis[80], G. Halimoglu[70], H. Hamagaki[85], G. Hamar[147], M. Hamid[7], R. Hannigan[121], M.R. Haque[144,89], A. Harlenderova[110], J.W. Harris[148], A. Harton[10], J.A. Hasenbichler[35], H. Hassan[99], D. Hatzifotiadou[55], P. Hauer[44], L.B. Havener[148], S. Hayashi[135], S.T. Heckel[108],

E. Hellbär[70], H. Helstrup[37], T. Herman[38], E.G. Hernandez[46], G. Herrera Corral[9], F. Herrmann[146], K.F. Hetland[37], H. Hillemanns[35], C. Hills[130], B. Hippolyte[139], B. Hofman[64], B. Hohlweger[93,108], J. Honermann[146], G.H. Hong[149], D. Horak[38], S. Hornung[110], A. Horzyk[2], R. Hosokawa[15], P. Hristov[35], C. Huang[80], C. Hughes[133], P. Huhn[70], T.J. Humanic[100], H. Hushnud[112], L.A. Husova[146], A. Hutson[127], D. Hutter[40], J.P. Iddon[35,130], R. Ilkaev[111], H. Ilyas[14], M. Inaba[136], G.M. Innocenti[35], M. Ippolitov[91], A. Isakov[38,98], M.S. Islam[112], M. Ivanov[110], V. Ivanov[101], V. Izucheev[94], M. Jablonski[2], B. Jacak[82], N. Jacazio[35], P.M. Jacobs[82], S. Jadlovska[119], J. Jadlovsky[119], S. Jaelani[64], C. Jahnke[124,123], M.J. Jakubowska[144], M.A. Janik[144], T. Janson[76], M. Jercic[102], O. Jevons[113], F. Jonas[99,146], P.G. Jones[113], J.M. Jowett[35,110], J. Jung[70], M. Jung[70], A. Junique[35], A. Jusko[113], J. Kaewjai[118], P. Kalinak[66], A. Kalweit[35], V. Kaplin[96], S. Kar[7], A. Karasu Uysal[79], D. Karatovic[102], O. Karavichev[65], T. Karavicheva[65], P. Karczmarczyk[144], E. Karpechev[65], A. Kazantsev[91], U. Kebschull[76], R. Keidel[48], D.L.D. Keijdener[64], M. Keil[35], B. Ketzer[44], Z. Khabanova[93], A.M. Khan[7], S. Khan[16], A. Khanzadeev[101], Y. Kharlov[94], A. Khatun[16], A. Khuntia[120], B. Kileng[37], B. Kim[17,63], D. Kim[149], D.J. Kim[128], E.J. Kim[75], J. Kim[149], J.S. Kim[42], J. Kim[107], J. Kim[149], J. Kim[75], M. Kim[107], S. Kim[18], T. Kim[149], S. Kirsch[70], I. Kisel[40], S. Kiselev[95], A. Kisiel[144], J.P. Kitowski[2], J.L. Klay[6], J. Klein[35], S. Klein[82], C. Klein-Bösing[146], M. Kleiner[70], T. Klemenz[108], A. Kluge[35], A.G. Knospe[127], C. Kobdaj[118], M.K. Köhler[107], T. Kollegger[110], A. Kondratyev[77], N. Kondratyeva[96], E. Kondratyuk[94], J. Konig[70], S.A. Konigstorfer[108], P.J. Konopka[35,2], G. Kornakov[144], S.D. Koryciak[2], L. Koska[119], A. Kotliarov[98], O. Kovalenko[88], V. Kovalenko[115], M. Kowalski[120], I. Králik[66], A. Kravčáková[39], L. Kreis[110], M. Krivda[113,66], F. Krizek[98], K. Krizkova Gajdosova[38], M. Kroesen[107], M. Krüger[70], E. Kryshen[101], M. Krzewicki[40], V. Kučera[35], C. Kuhn[139], P.G. Kuijer[93], T. Kumaoka[136], D. Kumar[143], L. Kumar[103], N. Kumar[103], S. Kundu[35,89], P. Kurashvili[88], A. Kurepin[65], A.B. Kurepin[65], A. Kuryakin[111], S. Kushpil[98], J. Kvapil[113], M.J. Kweon[63], J.Y. Kwon[63], Y. Kwon[149], S.L. La Pointe[40], P. La Rocca[27], Y.S. Lai[82], A. Lakrathok[118], M. Lamanna[35], R. Langoy[132], K. Lapidus[35], P. Larionov[53], E. Laudi[35], L. Lautner[35,108], R. Lavicka[38], T. Lazareva[115], R. Lea[142,24,59], J. Lee[136], J. Lehrbach[40], R.C. Lemmon[97], I. León Monzón[122], E.D. Lesser[19], M. Lettrich[35,108], P. Lévai[147], X. Li[11], X.L. Li[7], J. Lien[132], R. Lietava[113], B. Lim[17], S.H. Lim[17], V. Lindenstruth[40], A. Lindner[49], C. Lippmann[110], A. Liu[19], J. Liu[130], I.M. Lofnes[21], V. Loginov[96], C. Loizides[99], P. Loncar[36], J.A. Lopez[107], X. Lopez[137], E. López Torres[8], J.R. Luhder[146], M. Lunardon[28], G. Luparello[62], Y.G. Ma[41], A. Maevskaya[65], M. Mager[35], T. Mahmoud[44], A. Maire[139], M. Malaev[101], Q.W. Malik[20], L. Malinina[IV,77], D. Mal'Kevich[95], N. Mallick[51], P. Malzacher[110], G. Mandaglio[33,57], V. Manko[91], F. Manso[137], V. Manzari[54], Y. Mao[7], J. Mareš[68], G.V. Margagliotti[24], A. Margotti[55], A. Marín[110], C. Markert[121], M. Marquard[70], N.A. Martin[107], P. Martinengo[35], J.L. Martinez[127], M.I. Martínez[46], G. Martínez García[117], S. Masciocchi[110], M. Masera[25], A. Masoni[56], L. Massacrier[80], A. Mastroserio[141,54], A.M. Mathis[108], O. Matonoha[83], P.F.T. Matuoka[123], A. Matyja[120], C. Mayer[120], A.L. Mazuecos[35], F. Mazzaschi[25], M. Mazzilli[35], M.A. Mazzoni[60], J.E. Mdhluli[134], A.F. Mechler[70], F. Meddi[22], Y. Melikyan[65], A. Menchaca-Rocha[73], E. Meninno[116,30], A.S. Menon[127], M. Meres[13], S. Mhlanga[126,74], Y. Miake[136], L. Micheletti[61,25], L.C. Migliorin[138], D.L. Mihaylov[108], K. Mikhaylov[77,95], A.N. Mishra[147], D. Miśkowiec[110], A. Modak[4], A.P. Mohanty[64], B. Mohanty[89], M. Mohisin Khan[16], Z. Moravcova[92], C. Mordasini[108], D.A. Moreira De Godoy[146], L.A.P. Moreno[46], I. Morozov[65], A. Morsch[35], T. Mrnjavac[35], V. Muccifora[53], E. Mudnic[36], D. Mühlheim[146], S. Muhuri[143], J.D. Mulligan[82], A. Mulliri[23], M.G. Munhoz[123], R.H. Munzer[70], H. Murakami[135], S. Murray[126], L. Musa[35], J. Musinsky[66], C.J. Myers[127], J.W. Myrcha[144], B. Naik[134,50], R. Nair[88], B.K. Nandi[50], R. Nania[55], E. Nappi[54], M.U. Naru[14], A.F. Nassirpour[83], A. Nath[107], C. Nattrass[133], A. Neagu[20], L. Nellen[71], S.V. Nesbo[37], G. Neskovic[40], D. Nesterov[115], B.S. Nielsen[92], S. Nikolaev[91], S. Nikulin[91], V. Nikulin[101], F. Noferini[55], S. Noh[12], P. Nomokonov[77], J. Norman[130], N. Novitzky[136], P. Nowakowski[144], A. Nyanin[91], J. Nystrand[21], M. Ogino[85], A. Ohlson[83], V.A. Okorokov[96], J. Oleniacz[144], A.C. Oliveira Da Silva[133], M.H. Oliver[148], A. Onnerstad[128], C. Oppedisano[61], A. Ortiz Velasquez[71], T. Osako[47], A. Oskarsson[83], J. Otwinowski[120], K. Oyama[85], Y. Pachmayer[107], S. Padhan[50], D. Pagano[142,59], G. Paić[71], A. Palasciano[54], J. Pan[145], S. Panebianco[140], P. Pareek[143], J. Park[63], J.E. Parkkila[128], S.P. Pathak[127], R.N. Patra[104,35], B. Paul[23], J. Pazzini[142,59], H. Pei[7], T. Peitzmann[64], X. Peng[7], L.G. Pereira[72], H. Pereira Da Costa[140], D. Peresunko[91], G.M. Perez[8], S. Perrin[140], Y. Pestov[5], V. Petráček[38], M. Petrovici[49], R.P. Pezzi[72], S. Piano[62], M. Pikna[13], P. Pillot[117], O. Pinazza[55,35], L. Pinsky[127], C. Pinto[27], S. Pisano[53], M. Płoskoń[82], M. Planinic[102], F. Pliquett[70], M.G. Poghosyan[99], B. Polichtchouk[94], S. Politano[31], N. Poljak[102], A. Pop[49], S. Porteboeuf-Houssais[137], J. Porter[82], V. Pozdniakov[77], S.K. Prasad[4], R. Preghenella[55], F. Prino[61], C.A. Pruneau[145], I. Pshenichnov[65], M. Puccio[35], S. Qiu[93], L. Quaglia[25], R.E. Quishpe[127], S. Ragoni[113], A. Rakotozafindrabe[140], L. Ramello[32], F. Rami[139], S.A.R. Ramirez[46], A.G.T. Ramos[34], T.A. Rancien[81], R. Raniwala[105], S. Raniwala[105], S.S. Räsänen[45],

R. Rath[51], I. Ravasenga[93], K.F. Read[99,133], A.R. Redelbach[40], K. Redlich[V,88], A. Rehman[21], P. Reichelt[70], F. Reidt[35], H.A. Reme-ness[37], R. Renfordt[70], Z. Rescakova[39], K. Reygers[107], A. Riabov[101], V. Riabov[101], T. Richert[83,92], M. Richter[20], W. Riegler[35], F. Riggi[27], C. Ristea[69], S.P. Rode[51], M. Rodríguez Cahuantzi[46], K. Røed[20], R. Rogalev[94], E. Rogochaya[77], T.S. Rogoschinski[70], D. Rohr[35], D. Röhrich[21], P.F. Rojas[46], P.S. Rokita[144], F. Ronchetti[53], A. Rosano[33,57], E.D. Rosas[71], A. Rossi[58], A. Rotondi[29,59], A. Roy[51], P. Roy[112], S. Roy[50], N. Rubini[26], O.V. Rueda[83], R. Rui[24], B. Rumyantsev[77], P.G. Russek[2], A. Rustamov[90], E. Ryabinkin[91], Y. Ryabov[101], A. Rybicki[120], H. Rytkonen[128], W. Rzesa[144], O.A.M. Saarimaki[45], R. Sadek[117], S. Sadovsky[94], J. Saetre[21], K. Šafařík[38], S.K. Saha[143], S. Saha[89], B. Sahoo[50], P. Sahoo[50], R. Sahoo[51], S. Sahoo[67], D. Sahu[51], P.K. Sahu[67], J. Saini[143], S. Sakai[136], S. Sambyal[104], V. Samsonov[I,101,96], D. Sarkar[145], N. Sarkar[143], P. Sarma[43], V.M. Sarti[108], M.H.P. Sas[148], J. Schambach[99,121], H.S. Scheid[70], C. Schiaua[49], R. Schicker[107], A. Schmah[107], C. Schmidt[110], H.R. Schmidt[106], M.O. Schmidt[107], M. Schmidt[106], N.V. Schmidt[99,70], A.R. Schmier[133], R. Schotter[139], J. Schukraft[35], Y. Schutz[139], K. Schwarz[110], K. Schweda[110], G. Scioli[26], E. Scomparin[61], J.E. Seger[15], Y. Sekiguchi[135], D. Sekihata[135], I. Selyuzhenkov[110,96], S. Senyukov[139], J.J. Seo[63], D. Serebryakov[65], L. Šerkšnytė[108], A. Sevcenco[69], T.J. Shaba[74], A. Shabanov[65], A. Shabetai[117], R. Shahoyan[35], W. Shaikh[112], A. Shangaraev[94], A. Sharma[103], H. Sharma[120], M. Sharma[104], N. Sharma[103], S. Sharma[104], O. Sheibani[127], K. Shigaki[47], M. Shimomura[86], S. Shirinkin[95], Q. Shou[41], Y. Sibiriak[91], S. Siddhanta[56], T. Siemiarczuk[88], T.F. Silva[123], D. Silvermyr[83], G. Simonetti[35], B. Singh[108], R. Singh[89], R. Singh[104], R. Singh[51], V.K. Singh[143], V. Singhal[143], T. Sinha[112], B. Sitar[13], M. Sitta[32], T.B. Skaali[20], G. Skorodumovs[107], M. Slupecki[45], N. Smirnov[148], R.J.M. Snellings[64], C. Soncco[114], J. Song[127], A. Songmoolnak[118], F. Soramel[28], S. Sorensen[133], I. Sputowska[120], J. Stachel[107], I. Stan[69], P.J. Steffanic[133], S.F. Stiefelmaier[107], D. Stocco[117], I. Storehaug[20], M.M. Storetvedt[37], C.P. Stylianidis[93], A.A.P. Suaide[123], T. Sugitate[47], C. Suire[80], M. Suljic[35], R. Sultanov[95], M. Šumbera[98], V. Sumberia[104], S. Sumowidagdo[52], S. Swain[67], A. Szabo[13], I. Szarka[13], U. Tabassam[14], S.F. Taghavi[108], G. Taillepied[137], J. Takahashi[124], G.J. Tambave[21], S. Tang[137,7], Z. Tang[131], M. Tarhini[117], M.G. Tarzila[49], A. Tauro[35], G. Tejeda Muñoz[46], A. Telesca[35], L. Terlizzi[25], C. Terrevoli[127], G. Tersimonov[3], S. Thakur[143], D. Thomas[121], R. Tieulent[138], A. Tikhonov[65], A.R. Timmins[127], M. Tkacik[119], A. Toia[70], N. Topilskaya[65], M. Toppi[53], F. Torales-Acosta[19], T. Tork[80], R.C. Torres[82], S.R. Torres[38], A. Trifiró[33,57], S. Tripathy[55,71], T. Tripathy[50], S. Trogolo[35,28], G. Trombetta[34], V. Trubnikov[3], W.H. Trzaska[128], T.P. Trzcinski[144], B.A. Trzeciak[38], A. Tumkin[111], R. Turrisi[58], T.S. Tveter[20], K. Ullaland[21], A. Uras[138], M. Urioni[59,142], G.L. Usai[23], M. Vala[39], N. Valle[59,29], S. Vallero[61], N. van der Kolk[64], L.V.R. van Doremalen[64], M. van Leeuwen[93], R.J.G. van Weelden[93], P. Vande Vyvre[35], D. Varga[147], Z. Varga[147], M. Varga-Kofarago[147], A. Vargas[46], M. Vasileiou[87], A. Vasiliev[91], O. Vázquez Doce[108], V. Vechernin[115], E. Vercellin[25], S. Vergara Limón[46], L. Vermunt[64], R. Vértesi[147], M. Verweij[64], L. Vickovic[36], Z. Vilakazi[134], O. Villalobos Baillie[113], G. Vino[54], A. Vinogradov[91], T. Virgili[30], V. Vislavicius[92], A. Vodopyanov[77], B. Volkel[35], M.A. Völkl[107], K. Voloshin[95], S.A. Voloshin[145], G. Volpe[34], B. von Haller[35], I. Vorobyev[108], D. Voscek[119], J. Vrláková[39], B. Wagner[21], C. Wang[41], D. Wang[41], M. Weber[116], A. Wegrzynek[35], S.C. Wenzel[35], J.P. Wessels[146], J. Wiechula[70], J. Wikne[20], G. Wilk[88], J. Wilkinson[110], G.A. Willems[146], E. Willsher[113], B. Windelband[107], M. Winn[140], W.E. Witt[133], J.R. Wright[121], W. Wu[41], Y. Wu[131], R. Xu[7], S. Yalcin[79], Y. Yamaguchi[47], K. Yamakawa[47], S. Yang[21], S. Yano[47,140], Z. Yin[7], H. Yokoyama[64], I.-K. Yoo[17], J.H. Yoon[63], S. Yuan[21], A. Yuncu[107], V. Zaccolo[24], A. Zaman[14], C. Zampolli[35], H.J.C. Zanoli[64], N. Zardoshti[35], A. Zarochentsev[115], P. Závada[68], N. Zaviyalov[111], H. Zbroszczyk[144], M. Zhalov[101], S. Zhang[41], X. Zhang[7], Y. Zhang[131], V. Zherebchevskii[115], Y. Zhi[11], D. Zhou[7], Y. Zhou[92], J. Zhu[7,110], Y. Zhu[7], A. Zichichi[26], G. Zinovjev[3], N. Zurlo[142,59].

Affiliation notes

[I] Deceased

[II] Also at: Italian National Agency for New Technologies, Energy and Sustainable Economic Development (ENEA), Bologna, Italy

[III] Also at: Dipartimento DET del Politecnico di Torino, Turin, Italy

[IV] Also at: M.V. Lomonosov Moscow State University, D.V. Skobeltsyn Institute of Nuclear, Physics, Moscow, Russia

[V] Also at: Institute of Theoretical Physics, University of Wroclaw, Poland

Collaboration Institutes

[1] A.I. Alikhanyan National Science Laboratory (Yerevan Physics Institute) Foundation, Yerevan, Armenia

[2] AGH University of Science and Technology, Cracow, Poland

[3] Bogolyubov Institute for Theoretical Physics, National Academy of Sciences of Ukraine, Kiev, Ukraine

[4] Bose Institute, Department of Physics and Centre for Astroparticle Physics and Space Science (CAPSS), Kolkata, India

[5] Budker Institute for Nuclear Physics, Novosibirsk, Russia

[6] California Polytechnic State University, San Luis Obispo, California, United States

[7] Central China Normal University, Wuhan, China

[8] Centro de Aplicaciones Tecnológicas y Desarrollo Nuclear (CEADEN), Havana, Cuba

[9] Centro de Investigación y de Estudios Avanzados (CINVESTAV), Mexico City and Mérida, Mexico

[10] Chicago State University, Chicago, Illinois, United States

[11] China Institute of Atomic Energy, Beijing, China

[12] Chungbuk National University, Cheongju, Republic of Korea

[13] Comenius University Bratislava, Faculty of Mathematics, Physics and Informatics, Bratislava, Slovakia

[14] COMSATS University Islamabad, Islamabad, Pakistan

[15] Creighton University, Omaha, Nebraska, United States

[16] Department of Physics, Aligarh Muslim University, Aligarh, India

[17] Department of Physics, Pusan National University, Pusan, Republic of Korea

[18] Department of Physics, Sejong University, Seoul, Republic of Korea

[19] Department of Physics, University of California, Berkeley, California, United States

[20] Department of Physics, University of Oslo, Oslo, Norway

[21] Department of Physics and Technology, University of Bergen, Bergen, Norway

[22] Dipartimento di Fisica dell'Università 'La Sapienza' and Sezione INFN, Rome, Italy

[23] Dipartimento di Fisica dell'Università and Sezione INFN, Cagliari, Italy

[24] Dipartimento di Fisica dell'Università and Sezione INFN, Trieste, Italy

[25] Dipartimento di Fisica dell'Università and Sezione INFN, Turin, Italy

[26] Dipartimento di Fisica e Astronomia dell'Università and Sezione INFN, Bologna, Italy

[27] Dipartimento di Fisica e Astronomia dell'Università and Sezione INFN, Catania, Italy

[28] Dipartimento di Fisica e Astronomia dell'Università and Sezione INFN, Padova, Italy

[29] Dipartimento di Fisica e Nucleare e Teorica, Università di Pavia, Pavia, Italy

[30] Dipartimento di Fisica 'E.R. Caianiello' dell'Università and Gruppo Collegato INFN, Salerno, Italy

[31] Dipartimento DISAT del Politecnico and Sezione INFN, Turin, Italy

[32] Dipartimento di Scienze e Innovazione Tecnologica dell'Università del Piemonte Orientale and INFN Sezione di Torino, Alessandria, Italy

[33] Dipartimento di Scienze MIFT, Università di Messina, Messina, Italy

[34] Dipartimento Interateneo di Fisica 'M. Merlin' and Sezione INFN, Bari, Italy

[35] European Organization for Nuclear Research (CERN), Geneva, Switzerland

[36] Faculty of Electrical Engineering, Mechanical Engineering and Naval Architecture, University of Split, Split, Croatia

[37] Faculty of Engineering and Science, Western Norway University of Applied Sciences, Bergen, Norway

[38] Faculty of Nuclear Sciences and Physical Engineering, Czech Technical University in Prague, Prague, Czech Republic

[39] Faculty of Science, P.J. Šafárik University, Košice, Slovakia

[40] Frankfurt Institute for Advanced Studies, Johann Wolfgang Goethe-Universität Frankfurt, Frankfurt, Germany

[41] Fudan University, Shanghai, China

[42] Gangneung-Wonju National University, Gangneung, Republic of Korea

[43] Gauhati University, Department of Physics, Guwahati, India

[44] Helmholtz-Institut für Strahlen- und Kernphysik, Rheinische Friedrich-Wilhelms-Universität Bonn, Bonn, Germany

[45] Helsinki Institute of Physics (HIP), Helsinki, Finland

[46] High Energy Physics Group, Universidad Autónoma de Puebla, Puebla, Mexico

[47] Hiroshima University, Hiroshima, Japan

[48] Hochschule Worms, Zentrum für Technologietransfer und Telekommunikation (ZTT), Worms, Germany

[49] Horia Hulubei National Institute of Physics and Nuclear Engineering, Bucharest, Romania

[50] Indian Institute of Technology Bombay (IIT), Mumbai, India

[51] Indian Institute of Technology Indore, Indore, India

[52] Indonesian Institute of Sciences, Jakarta, Indonesia

[53] INFN, Laboratori Nazionali di Frascati, Frascati, Italy

[54] INFN, Sezione di Bari, Bari, Italy

[55] INFN, Sezione di Bologna, Bologna, Italy

[56] INFN, Sezione di Cagliari, Cagliari, Italy

[57] INFN, Sezione di Catania, Catania, Italy

[58] INFN, Sezione di Padova, Padova, Italy

[59] INFN, Sezione di Pavia, Pavia, Italy

[60] INFN, Sezione di Roma, Rome, Italy

[61] INFN, Sezione di Torino, Turin, Italy

[62] INFN, Sezione di Trieste, Trieste, Italy

[63] Inha University, Incheon, Republic of Korea

[64] Institute for Gravitational and Subatomic Physics (GRASP), Utrecht University/Nikhef, Utrecht, Netherlands

[65] Institute for Nuclear Research, Academy of Sciences, Moscow, Russia

[66] Institute of Experimental Physics, Slovak Academy of Sciences, Košice, Slovakia

[67] Institute of Physics, Homi Bhabha National Institute, Bhubaneswar, India

[68] Institute of Physics of the Czech Academy of Sciences, Prague, Czech Republic

[69] Institute of Space Science (ISS), Bucharest, Romania

[70] Institut für Kernphysik, Johann Wolfgang Goethe-Universität Frankfurt, Frankfurt, Germany

[71] Instituto de Ciencias Nucleares, Universidad Nacional Autónoma de México, Mexico City, Mexico

[72] Instituto de Física, Universidade Federal do Rio Grande do Sul (UFRGS), Porto Alegre, Brazil

[73] Instituto de Física, Universidad Nacional Autónoma de México, Mexico City, Mexico

[74] iThemba LABS, National Research Foundation, Somerset West, South Africa

[75] Jeonbuk National University, Jeonju, Republic of Korea

[76] Johann-Wolfgang-Goethe Universität Frankfurt Institut für Informatik, Fachbereich Informatik und Mathematik, Frankfurt, Germany

[77] Joint Institute for Nuclear Research (JINR), Dubna, Russia

[78] Korea Institute of Science and Technology Information, Daejeon, Republic of Korea

[79] KTO Karatay University, Konya, Turkey

[80] Laboratoire de Physique des 2 Infinis, Irène Joliot-Curie, Orsay, France

[81] Laboratoire de Physique Subatomique et de Cosmologie, Université Grenoble-Alpes, CNRS-IN2P3, Grenoble, France

[82] Lawrence Berkeley National Laboratory, Berkeley, California, United States

[83] Lund University Department of Physics, Division of Particle Physics, Lund, Sweden

[84] Moscow Institute for Physics and Technology, Moscow, Russia

[85] Nagasaki Institute of Applied Science, Nagasaki, Japan

[86] Nara Women's University (NWU), Nara, Japan

[87] National and Kapodistrian University of Athens, School of Science, Department of Physics , Athens, Greece

[88] National Centre for Nuclear Research, Warsaw, Poland

[89] National Institute of Science Education and Research, Homi Bhabha National Institute, Jatni, India

[90] National Nuclear Research Center, Baku, Azerbaijan

[91] National Research Centre Kurchatov Institute, Moscow, Russia

[92] Niels Bohr Institute, University of Copenhagen, Copenhagen, Denmark

[93] Nikhef, National institute for subatomic physics, Amsterdam, Netherlands

[94] NRC Kurchatov Institute IHEP, Protvino, Russia

[95] NRC «Kurchatov»Institute - ITEP, Moscow, Russia

[96] NRNU Moscow Engineering Physics Institute, Moscow, Russia

[97] Nuclear Physics Group, STFC Daresbury Laboratory, Daresbury, United Kingdom

[98] Nuclear Physics Institute of the Czech Academy of Sciences, Řež u Prahy, Czech Republic

[99] Oak Ridge National Laboratory, Oak Ridge, Tennessee, United States

[100] Ohio State University, Columbus, Ohio, United States

[101] Petersburg Nuclear Physics Institute, Gatchina, Russia

[102] Physics department, Faculty of science, University of Zagreb, Zagreb, Croatia

[103] Physics Department, Panjab University, Chandigarh, India

[104] Physics Department, University of Jammu, Jammu, India

[105] Physics Department, University of Rajasthan, Jaipur, India

[106] Physikalisches Institut, Eberhard-Karls-Universität Tübingen, Tübingen, Germany

[107] Physikalisches Institut, Ruprecht-Karls-Universität Heidelberg, Heidelberg, Germany

[108] Physik Department, Technische Universität München, Munich, Germany

[109] Politecnico di Bari and Sezione INFN, Bari, Italy

[110] Research Division and ExtreMe Matter Institute EMMI, GSI Helmholtzzentrum für Schwerionenforschung GmbH, Darmstadt, Germany

[111] Russian Federal Nuclear Center (VNIIEF), Sarov, Russia

[112] Saha Institute of Nuclear Physics, Homi Bhabha National Institute, Kolkata, India

[113] School of Physics and Astronomy, University of Birmingham, Birmingham, United Kingdom

[114] Sección Física, Departamento de Ciencias, Pontificia Universidad Católica del Perú, Lima, Peru

[115] St. Petersburg State University, St. Petersburg, Russia

[116] Stefan Meyer Institut für Subatomare Physik (SMI), Vienna, Austria

[117] SUBATECH, IMT Atlantique, Université de Nantes, CNRS-IN2P3, Nantes, France

[118] Suranaree University of Technology, Nakhon Ratchasima, Thailand

[119] Technical University of Košice, Košice, Slovakia

[120] The Henryk Niewodniczanski Institute of Nuclear Physics, Polish Academy of Sciences, Cracow, Poland

[121] The University of Texas at Austin, Austin, Texas, United States

[122] Universidad Autónoma de Sinaloa, Culiacán, Mexico

[123] Universidade de São Paulo (USP), São Paulo, Brazil

[124] Universidade Estadual de Campinas (UNICAMP), Campinas, Brazil

[125] Universidade Federal do ABC, Santo Andre, Brazil

[126] University of Cape Town, Cape Town, South Africa

[127] University of Houston, Houston, Texas, United States

[128] University of Jyväskylä, Jyväskylä, Finland

[129] University of Kansas, Lawrence, Kansas, United States

[130] University of Liverpool, Liverpool, United Kingdom

[131] University of Science and Technology of China, Hefei, China

[132] University of South-Eastern Norway, Tonsberg, Norway

[133] University of Tennessee, Knoxville, Tennessee, United States

[134] University of the Witwatersrand, Johannesburg, South Africa

[135] University of Tokyo, Tokyo, Japan

[136] University of Tsukuba, Tsukuba, Japan

[137] Université Clermont Auvergne, CNRS/IN2P3, LPC, Clermont-Ferrand, France

[138] Université de Lyon, CNRS/IN2P3, Institut de Physique des 2 Infinis de Lyon , Lyon, France

[139] Université de Strasbourg, CNRS, IPHC UMR 7178, F-67000 Strasbourg, France, Strasbourg, France

[140] Université Paris-Saclay Centre d'Etudes de Saclay (CEA), IRFU, Départment de Physique Nucléaire (DPhN), Saclay, France

[141] Università degli Studi di Foggia, Foggia, Italy

[142] Università di Brescia, Brescia, Italy

[143] Variable Energy Cyclotron Centre, Homi Bhabha National Institute, Kolkata, India

[144] Warsaw University of Technology, Warsaw, Poland

[145] Wayne State University, Detroit, Michigan, United States

[146] Westfälische Wilhelms-Universität Münster, Institut für Kernphysik, Münster, Germany

[147] Wigner Research Centre for Physics, Budapest, Hungary

[148] Yale University, New Haven, Connecticut, United States

[149] Yonsei University, Seoul, Republic of Korea